X-ray Jets

Aneta Siemiginowska

The Active Galaxy 4C+29.30

Credit: X-ray: NASA/CXC/SAO/A.Siemiginowska et al;
Optical: NASA/STScI; Radio: NSF/NRAO/VLA

Contents

X-ray Jets

Aneta Siemiginowska

The first recorded observation of an extragalactic jet was made almost a century ago. In 1918 Heber Curtis, an astronomer in the Lick Observatory, published "Descriptions of 762 nebulae and clusters photographed with the Crossley Reflector." He wrote a note by the entry for NGC 4486 (M87): "*A curious straight ray lies in a gap in the nebulosity in p.a. 20 deg apparently connected with the nucleus by a thin line of matter. The ray is brightest at its inner end, which is 11 arcsec from the nucleus.*"

A few decades later Baade & Minkowski (1954) published an optical image of M87 showing 20 arcsec long and 2 arcsec wide jet with clear condensations along the jet. It is surprising to read their statement: "*No possibility exists at this time of forming any hypothesis on the formation of the jet, the physical state of its material, and the mechanism which connects the existence of the jet with the observed radio emission.*"

This was 1954, the era of pre-digital astronomy, when image analysis was based on photographic plates and performed by eye, with a ruler and a pencil. Only a few radio sources had been identified at that time, quasars had yet to be discovered, and a few more decades had to lapse before the first X-ray observations of jets. The Einstein High Resolution Imager (HRI) provided the first X-ray data of M87 jet (Feigelson 1980; Schreier et al. 1982). The first jet discovered in X-rays was the jet of a radio galaxy Centaurus A which was later studied in radio wavelengths (Schreier et al. 1979). The Einstein HRI image of the famous quasar 3C273 needed careful analyses to discern X-rays emitted by the relativistic jet (Willingale 1981). Later on ROSAT provided a few more detections of jets, but only with *Chandra* did X-ray studies of large scale jets become routine.

During the past 15 years the *Chandra* X-ray Observatory has performed many observations of jets in a variety of objects, from stellar types in our galaxy to quasars in the high redshift universe. Understanding jets might bring us closer to understanding the physics of accreting systems across many different scales. While the observational data gathered over these past years underlined the significance of jets in the evolution of galaxies and clusters of galaxies, there are still many unanswered questions, including the nature of relativistic jets, jet energetics, particle content, particle acceleration and emission processes. Both statistical studies of large samples of jets across the entire electromagnetic spectrum and deep broad-band images of individual jets are necessary to tackle some of these questions.

In the *Chandra* Newsletter #13 (2006) Schwartz and Harris introduced the studies of X-ray jets which became possible with the high angular resolution X-ray mirrors provided by *Chandra*. Most of the X-ray jets remain unresolved in *XMM-Newton* or *Suzaku* observations and *Chandra* is critical to all the high angular resolution observations revealing the X-ray structures on sub-arcsec scales. In this letter I highlight some recent results of extragalactic jet studies with *Chandra* and direct the readers to more detailed reviews of the field given by Harris & Krawczynski (2006), Worrall (2009), and Pudritz et al. (2012).

Chandra Observations

The many discoveries of X-ray jets thrilled scientists in the early days of *Chandra*. They included the discovery of the PKS 0637-752 (Tavecchio et al. 2000, Cellotti et al. 2001, Schwartz et al. 2000) jet in the first calibration observation designed to test the focus of the mirrors on orbit. The initial discoveries were followed by a few systematic surveys to find X-ray jets and also by detailed studies of a few jets. The X-ray jets are seen as diffuse linear and bending structures with enhancements due to knots or hot spots. The jet is often located close to the strong core emission, or embedded in the diffuse emission of a host galaxy with a total length rarely exceeding $\sim 30''$. Most X-ray jets are rather faint and their emission is only a small ($< 3\%$) fraction of a strong core, the main reason why only a few jets were detected in earlier X-ray missions. *Chandra* opened a new window to the studies of relativistic extragalactic jets.

Several surveys of X-ray jets have been completed to date. They differ in their selection criteria, but all originated from samples of known radio jets. Sambruna et al. (2004) selected 17 radio jets from a list of known AGN jets. These radio jets were longer than $3''$ and bright ($S_{1.4GHz} > 5$mJy arcsec^{-2}), with at least one knot located at a large distance from the nucleus. The sample of Marshall et al. (2011) contained 56 flat spectrum radio quasars compiled from VLA and ATCA

imaging radio surveys and selected targets based on the flux density in the extended emission and the radio jet morphology. This sample was divided into two sub-classes: A – purely jet flux limited and B – based on radio morphology and biased toward one-sided and linear structure. In both surveys the *Chandra* observations were short (< 10 ksec), but about 60% of these radio jets were detected in X-rays. A higher fraction of resolved X-ray jets, 78%, in similar *Chandra* exposures was found by Hogan et al. (2011) in a sample of 13 blazars selected from the flux-limited MOJAVE sample of relativistic jets associated with quasars and FR II radio galaxies.

Most of the survey studies focused on understanding the X-ray emission process in large scale extragalactic jets. The possible mechanisms include synchrotron emission from highly relativistic particles in the jet or the emission resulting from the inverse Compton process where such particles transfer energy to lower frequency photons (radio-IR-optical-UV)

resulting in the X-ray emission. The source of the photon field could be internal to the jet (synchrotron-self-Compton, SSC) or external to the jet. In the large scale jets associated with quasars, the Cosmic Microwave Background was considered as the likely primary source of the photon field (IC/CMB).

Current observations indicate that synchrotron emission is the primary process producing X- rays in jets associated with low power radio galaxies classified as FRI. M87 and Centaurus A are examples of nearby FRI galaxies where the jets were studied in great detail. Both jets exhibit a correlated morphology (see M87 Fig. 1). The simple "one-zone" model where the radio and X-ray emission are produced by the same population of relativistic particles is supported by the observations. However, some evolution of the electron energy spectrum along the jet is required for these two cases. Recent studies of the archival *Chandra* data of FRI jets by Harwood & Hardcastle (2012) indicate no statistically significant correlations between the properties of the host galaxy and the jet, but show that the luminosity of X-ray jets scales linearly with the jet radio luminosity and that the X-ray spectral slope is related to both X-ray and radio luminosity of the jet. Since the X-ray emission in these jets is due to synchrotron processes, the particle acceleration mechanisms could be tested, but the sample of the suitable FRI jets is still limited.

Harris, Massaro and Cheung compiled a list of all X-ray jets detected with *Chandra* and made the radio and X-ray data available on the web page: http://hea-www.harvard.edu/XJET/. They (Massaro et al. 2011) used these data to describe statistical properties of all the detected X-ray jet features, knots, hot spots, diffuse jet emission. The archival sample is heterogeneous, consists of 106 sources (FRI and FRII radio galaxies and quasars) and shows
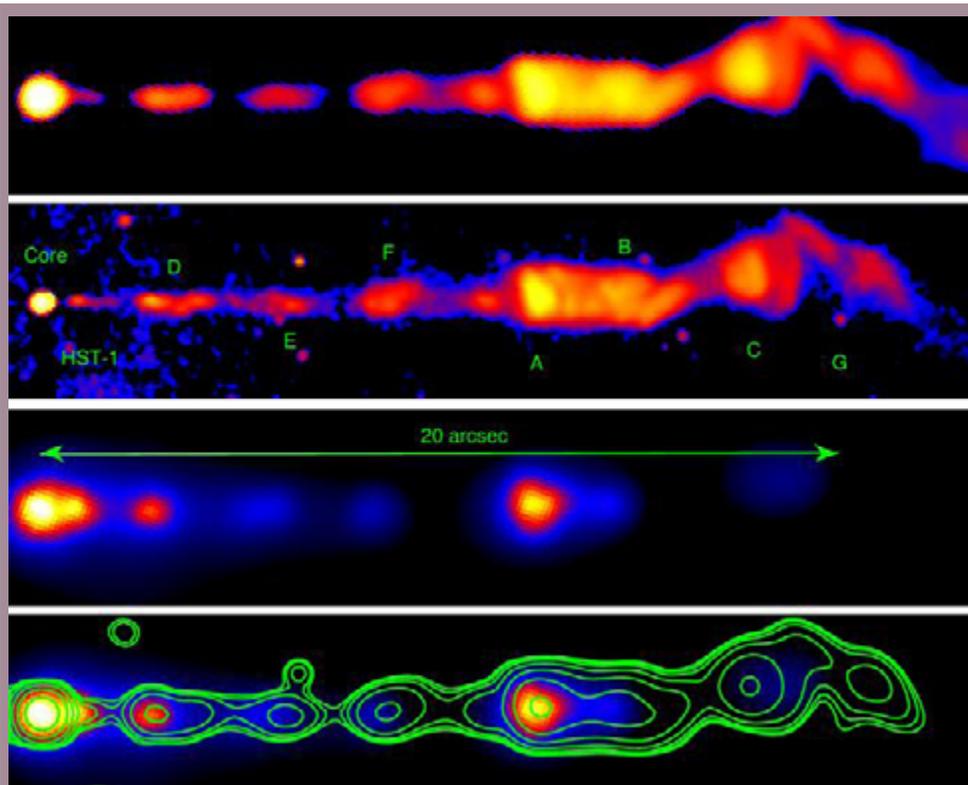
Fig. 1 — M87 jet in three bands, rotated to be horizontal (from Marshall et al. (2002)). Top: VLA image at 14.435 GHz with spatial resolution ~ 0.2″. Second panel: The HST Planetary Camera image in the F814W filter from Perlman et al. (2001). Third panel: Adaptively smoothed Chandra X-ray image. Lower panel: Smoothed Chandra image overlaid with contours of a Gaussian smoothed HST image matching the Chandra PSF. The HST and VLA images have a logarithmic stretch to bring out faint features, while the X-ray image scaling is linear.

a total of 236 detected jet related features. The redshift coverage at $z < 1$ is relatively good, but there are only a few sources at $z > 2$. This sample represents a variety of radio sources with X-ray jets in the *Chandra* archives to date. The statistical studies are still limited to small numbers and basic questions about the X-ray emission process or particle acceleration remain unanswered. However, there are interesting results indicating a real difference in the radio to X-ray flux ratios between the hotspots and knots in FRII sources (see 3C353 in Fig. 8), and no significant difference in the ratios for the knots in FRI and quasar jets. This second result suggests that either the knots in both types of jets are due to the synchrotron process, or that the inverse Compton process in quasar knots has very specific conditions resulting in the same flux ratios. A large sample of quasar jets, especially at high-z is needed to address these issues.

Quasar Jet Power

The total jet power, i.e. integrated over the entire lifetime of the jet, has been measured via X-ray cavities in X-ray clusters. This power can suppress cluster cooling and is therefore critical to the evolution of such structures in the universe. However, the instantaneous jet power carries the details of the jet launching physics yet is much harder to assess. The history of jet formation is imprinted into the jet X-ray emission, but is difficult to read unless we understand the primary emission processes in the jet. If the X-ray emission of quasar jets is predominantly due to inverse Compton scattering of the CMB, then under certain assumptions the bulk motion of the jet could be measured. High quality *Chandra* data with additional multiband radio and optical data are necessary to constrain the models (see, for example, Cara et al. 2013).

There have been only a few high quality deep *Chandra* observations of large scale quasar jets allowing detailed studies of evolution along the jet. One example was the jet in PKS 1127-145 (Fig. 2), a radio loud quasar at $z = 1.18$ (Siemiginowska et al. 2007). This jet shows a complex X-ray morphology and substructure within the knots. The X-ray and radio intensity profiles along the jet are quite different, with the radio peaking at the outermost regions of the jets and X-ray emission being strongest in the regions close to the quasar core. "One-zone" emission models fail; at least two components are needed to
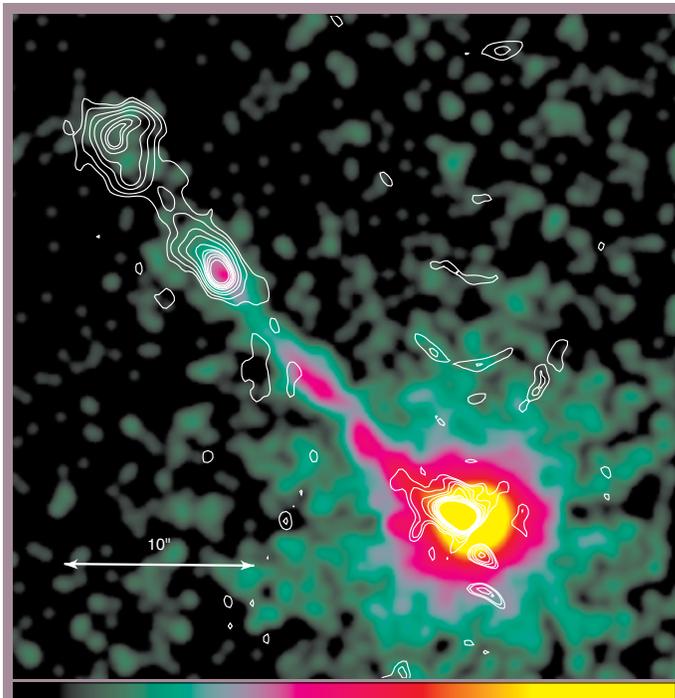

Fig. 2 — PKS 1127-125 (z = 1.118) image from Siemiginowska et al. (2007). The color scale is the smoothed Chandra *ACIS-S image showing a quasar with a jet of the ~ 300 kpc projected length. The contours are from the VLA 8.4 GHz image. The arrows indicate a 10" scale.*

explain the observations, with the X-rays originating in the proper relativistic jet, and the radio in a surrounding "sheath." The jet in 3C273 shows a similar behavior. Yet some jets, for example PKS 2101-490 (Godfrey et al. 2012a), show the opposite behavior, with the stronger X-rays at the end of a jet. For some other cases, radio and X-ray emission profiles have an almost constant intensity ratio along the jet, typically seen in FR I jets with the X-rays due to the synchrotron emission (Fig. 1). In addition, recent studies of PKS 0637-752 archival data by Godfrey et al. (2012b) revealed a quasi-periodic structure of the jet profile, suggesting a possible modulation in the jet launching process or a presence of re-confinement shocks. Estimates of the jet instantaneous power depend on the true process responsible for these observational trends seen by *Chandra*.

The high quality *Chandra* data indicate the complexity of quasar jets and of the physics responsible for powering jets, and the energy release. These data show that extragalactic jets remain relativistic out to large ~ Mpc distances from their origin, setting timescales for the jet activity stage in the evolving black hole. Important questions related to the physics of

particle acceleration at such large distances from the black hole remain unanswered.

Quasar Jets at High Redshift

Only a handful of high redshift quasar jets has been studied with *Chandra*. The highest redshift X-ray jets to date have been detected in luminous radio quasars, GB 1508+5714 ($z = 4.3$, Siemiginowska et al. 2003) and GB 1428+4217 ($z = 4.72$, Cheung et al. 2012). The *Chandra* images are not very impressive, showing only 3″–4″extension on one side of the quasar core with a small number of X-ray counts associated with the radio jets (see Fig. 3). The energy density of the CMB scales as $(1 + z)^4$ and in the simplest IC/CMB scenario, large scale jets with similar Lorentz factors should have the same surface brightness at any redshift (Schwartz 2002). However, this has not been observed; the high-z jets are fainter than these predictions. In fact, assuming the IC/CMB model, the Doppler factor derived for the two $z > 4$ jets of $\delta \sim 3$–6 is lower than observed in low-z jets. This suggests that the high-z jets might be intrinsically less relativistic or they decelerate more rapidly out to $\sim 10s$–$100s$ kpc scale than the low-z ones.

The current *Chandra* results for high-z jets are puzzling, but they are based on a just few observations. While most of the X-ray jets studied so far are located at $z < 2$, the highest redshift observations provide the most stringent test of the IC/CMB model. Future *Chandra* observations of a larger sample of kpc-scale radio jets over a broad redshift range at $z > 2$ are necessary. Such data should provide more insights to the jet physics and allow us to study the jets resulting from the "earliest" actively accreting black hole systems.

X-ray Variability of Jets

Jets are expected to vary. The parsec-scale blazar jets unresolved in X-rays show large amplitude flares across the entire electromagnetic spectrum. However, the variations of the larger scale X-ray resolved jet features have only been studied in a few jets with multiple *Chandra* observations.

The best X-ray monitoring data has been collected for the M87 jet, which was observed with *Chandra* more than 60 times between 2002–2008 (Harris et al. 2009) showing the most dramatic flux variability of the HST-1 knot. Initially the X-ray flux of the HST-1 knot increased by a factor of 2 in 116 days in 2002 and the knot faded over several months, but then again in 2005 the X-ray flux increased by a factor of ~ 50. The 2005 HST-1 flare was monitored by the HST and VLA. These data allowed for multi-frequency studies of the rise and decay times to constrain the emission size and the energy losses of the relativistic electrons. Harris et al. (2009) described details of these studies and concluded that the multi-frequency lightcurves are consistent with E^2 energy losses dominated by synchrotron cooling and yields an average magnetic field strength of 0.6 mG for the knot. Most surprising was the discovery of flux oscillation on a 0.5–0.8 year timescale. The origin of the oscillation remained unidentified, but Harris et al. (2009) suggested that it can be related to quasi-periodic variations in the conversion of the jet kinetic power to the internal energy of the radiating plasma. The HST-1 X-ray flare remains the strongest observed for a knot at a large distance (> 50 pc) from a supermassive black hole. While the X-ray flare of HST-1 happened on timescales longer than a year, the X-ray light-
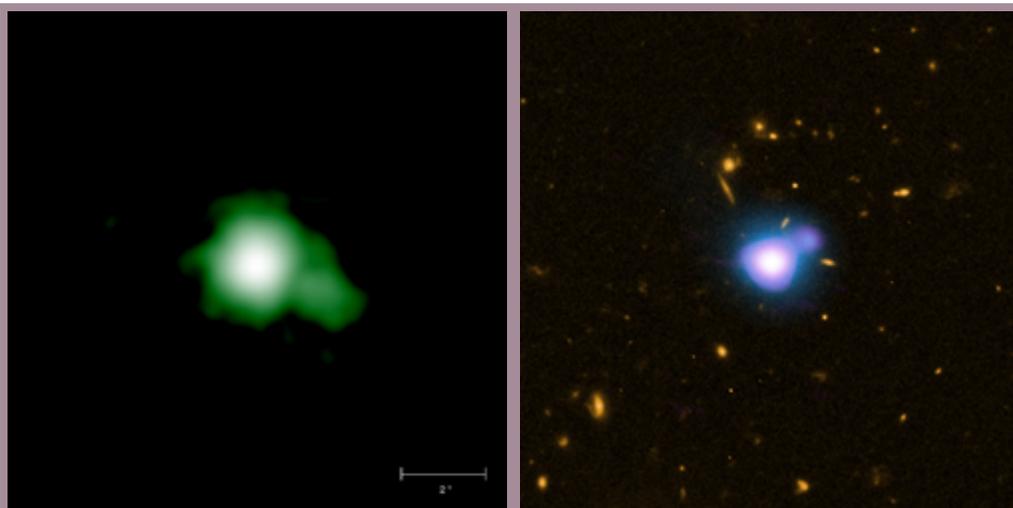

Fig. 3 — The two highest redshift quasar jets detected by Chandra *to date. Left: A smoothed* Chandra *image of the quasar GB 1508+5714 and its jet at* z = 4.3. *Right: A combined multiband image of GB 1428+4217 quasar and jet at* z = 4.72 : *X-rays are represented as blue, the optical HST as yellow and radio VLA image as purple.*
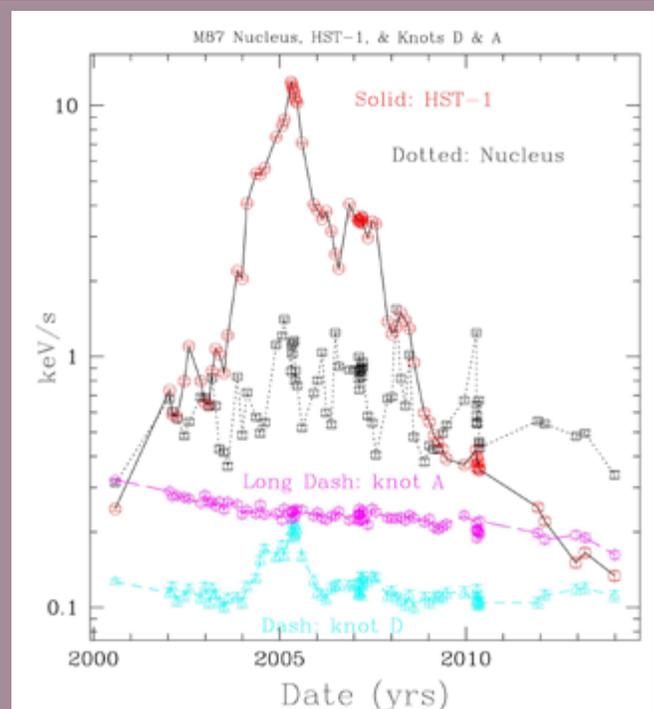
Fig. 4 — X-ray lightcurve of M87 nucleus and three knots HST-1, A, D collected over 13 years of Chandra monitoring program led by Dan Harris (Harris et al. 2009). A strong and long-lasting outburst of HST-1 knot dominates the lightcurve. The nucleus shows the short-term variability during the same time. During the time HST-1 was peaking, severe pileup corrupted the PSF so that both the nucleus and knot D photometric apertures were collecting a fraction of HST-1 events.

curve of the nucleus shows a short-term large fractional variability characteristic of the "flickering" suggesting that the TeV flare observed in 2005 may have originated in the nucleus. Monitoring of the M87 jet continues and the future observations should give answers to the critical question about the origin of the large amplitude short-term TeV flare, with important implications for our understanding of the physics associated with the accreting black hole and the relativistic jets.

The galaxy Centaurus A is a factor of ~ 2.5 closer than M87 and *Chandra* data resolved Centaurus A jet into more than 40 knots. Some of these knots have corresponding radio emission, but there are also knots with no radio counterpart. Many observations performed over the timescale of the mission allowed for detailed studies of the individual knots including proper motion, spectra and variability. Goodger et al. (2010) ruled out impulsive particle acceleration as a formation mechanism for the

knots and found no evidence for X-ray flux variability. The most likely mechanism for the stationary knots could be a collision resulting in a local shock followed by stable particle acceleration and X-ray synchrotron emission. An apparent motion in three knots was also detected, but there was no conclusive evidence for or against a faster moving "spine" within the jet.

The X-ray variability of high power large scale jets associated with quasars and FRII radio galaxies has not been studied in a systematic way. The knots in these powerful jets are larger and less resolved than in the two nearby FRI radio galaxies that have been monitored. Larger knots mean longer characteristic timescales. Only a small number of quasar jets have been observed more than once with *Chandra* during the last 15 years. The famous 3C273 quasar jet has several observations in the archives, but the variability analysis by Jester et al. (2006) did not show any significant changes in the X-ray knots. The only reported variability of the X-ray knot located at a large distance from the nucleus was in Pictor A (Marshall et
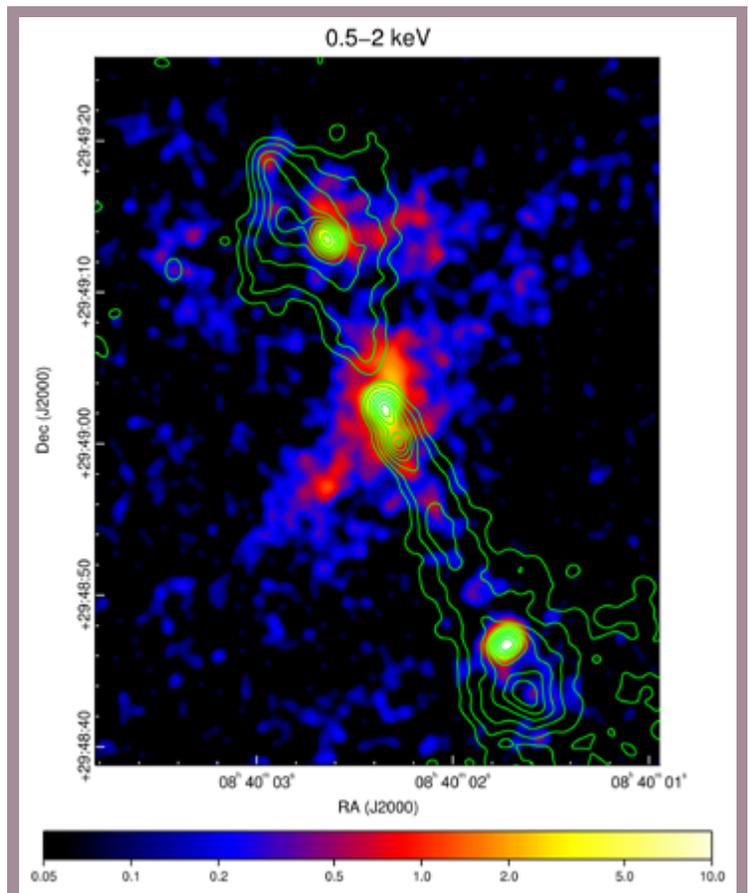

Fig. 5 — 4C+29.30 X-ray image with radio contours from Siemiginowska et al. (2012). Compare to the multiband composite image on the cover of this Newsletter.

al. 2010), where the X-ray knot disappeared between the *Chandra* observations of 2000 and 2002. Pictor A is a FRII radio galaxy with the projected jet length of about 150 kpc. An X-ray flare of the knot located $\sim 35''$ from the core is a surprise. Given the times-cales of the synchrotron losses, the size of the flaring region must be significantly smaller than the knot and characterized by a much larger magnetic field than the average over the entire jet. *Chandra* follow-up obser-vations of Pictor A should provide some more insight to the behavior of this knot.

Jet Impact on the ISM

The cover of this Newsletter issue displays a multi-band image showing complex morphology re-sulting from the jet outflow in a nearby elliptical gal-axy 4C+29.30 ($z = 0.0649$). 4C+29.30 could be viewed as an analog to the famous radio galaxy Centaurus A, but more distant and more powerful in the radio. It displays a similar morphology with a pronounced dust lane and cold gas stretching across the galaxy, perpen-dicular to the radio source axis. The 4C+29.30 radio source extends ~ 30 kpc from the center of the galaxy, showing a prominent one-sided jet but with lobes both south and north. The galaxy contains a strong extend-ed optical emission-line region at a similar distance from the center located at the edge of the elliptical gal-axy. The *Chandra* deep image shows complex X-ray emission spanning about ~ 60 kpc in total extent, marked by a pronounced center and two bright com-ponents coincident with the jet termination regions

Fig. 6 — *The interacting jet of the radio galaxy 3C305 (z = 0.0416). A composite multiband image shows smoothed* Chandra *X-rays in orange, radio in blue, and optical in green (Hardcastle et al. 2012).*

Fig. 7 — *The interacting jet of the radio galaxy 3C321. A composite multiband image shows X-ray data from* Chandra *(purple), optical and ultraviolet (UV) data from HST (red and orange), and radio from the VLA and MERLIN (blue). A bright, blue spot in the VLA and MERLIN radio image shows where the jet has struck the side of the galaxy and dissipates some energy. The jet is disrupted and deflected by this impact with the compan-ion galaxy (Evans et al. 2008).*

(the radio "hotspots," See Fig. 5). Faint diffuse X-ray emission traces the jet and connects the two hotspots, but extends beyond the radio emitting regions and shows several filaments. The bright X-rays north of the nucleus overlap with the clouds of line-emitting gas. There is also diffuse emission perpendicular to the jet axis across the center. so that the X-ray image gives an overall impression of an X-shaped structure.

The *Chandra* observation of 4C+29.30 contrib-utes to studies of the physics of radio source interac-tions with the ISM. This deep X-ray image allowed us to assess the overall energetics of the system with detail much-improved over the earlier studies in the radio and optical bands. The spectral analysis carried out for several of the brightest X-ray features indi-cated a mixture of thermal and non-thermal emission components, characterized by a variety of tempera-tures and spectral slopes. Possible variations in metal abundances of the hot ISM were also detected with high abundances in the center and the very low values (< 0.1 of the Solar) in the outer regions of the galaxy. The X-ray emission of the jet and the hotspots seems to be particularly complex, with different and distinct emission components, both thermal and non-thermal (synchrotron and/or inverse-Compton). The synchro-tron model for the X-ray jet is favored, but there are

large uncertainties and higher quality data are required for a statistically significant result.

It is in any case evident that a significant fraction of the jet energy (jet power, $L_j \sim 10^{42}$ erg s^{-1}) goes into heating the surrounding gas and the X-ray data support the heating of the ambient medium via weak shocks (Mach number M = 1.6). Only a small amount of the jet power is needed to accelerate clouds of colder material that are dragged along the outflow. The nucleus of the galaxy is surprisingly powerful in X-rays ($\sim 10^{44}$ erg s^{-1}) and heavily obscured by a significant amount of matter ($N_H \sim 5 \times 10^{23}$ cm^{-2}) falling towards the center (also indicated by HI absorption lines) (Sobolewska et al. 2012). This infall may be related to the feeding of the nucleus and triggering the current jet activity. The nucleus is sufficiently luminous to photo-ionize the whole extended emission-line region. These results support and strengthen conclusions regarding the feedback process operating in 4C+29.30 (Siemiginowska et al. 2012).

The direct impact of the jet on the interstellar medium in galaxies is evident. Details of jet-ISM interactions can be traced in several deep *Chandra* observations including M87 (Million et al. 2010), Cen A (Hardcastle et al. 2007) and a nearby Seyfert 1 galaxy NGC 4151 (Wang et al. 2011). Many observations indicate the presence of jet-induced outflow associated with optically emitting clouds. The signatures of a jet-induced shock with relatively low Mach number capable of heating the gas are also found in a few galaxies (see for example Fig. 6 and 7), providing strong evidence for the jet impact on the ISM and the importance of jets for the evolution of galaxies.

Summary and Future Perspectives

Chandra has initiated the X-ray studies of extragalactic jets. The first 15 years of *Chandra* observations indicate that jet X-ray emission is universal and that most jets can be detected in high spatial resolution X-ray observations of sufficient depth. The jet physics highlighted by the *Chandra* studies is complex, but the current high quality data have already provided important constraints on the emission process and on particle acceleration in radio galaxies. There are, however, many outstanding questions born from the *Chandra* observations and related to the energetics, particle acceleration and emission processes in powerful quasar jets. A few deep studies show that the jet morphology is complex, with fast and slow moving regions, and compact knots embedded in the more uniform diffuse emission. Signatures of complex interaction with the environment are seen in many observations of nearby jets, giving some early constraints on jet lifetime and evolution. More *Chandra* observations of jets are necessary to provide good statistical samples for studies of jets in general. The archival legacy of *Chandra* continues to be one of the most important goals in this field. With no new high angular resolution X-ray mission planned for the near future, *Chandra* remains our only choice for the X-ray studies of jets.

Fig. 8 — A composite image of 3C353 (z = 0.0304), an FR II radio galaxy: radio VLA (yellow) and Chandra *X-rays (blue). Two broad jets, hotspots and lobes are visible in the radio band. X-ray emission is detected in most radio structures: the nucleus, the jet and the counterjet, the terminal jet regions (hotspots), and one radio lobe. The X-rays associated with the knots and counterknots are inconsistent with the IC/CMB emission models (Kataoka et al. 2008).*

References

Baade, W., & Minkowski, R. 1954, ApJ, 119, 215

Cara, M., et al., 2013, ApJ, 773, 186

Celotti, A., Ghisellini, G., & Chiaberge, M., 2001, MNRAS, 321, L1

Cheung, C. C., Stawarz, Ł., Siemiginowska, A., et al. 2012, ApJ, 756, L20

Evans, D. A., Fong, W. F., Hardcastle, M. J., et al. 2008, ApJ, 675, 1057.

Feigelson, E. D. 1980, Ph.D. Thesis

Godfrey, L. E. H., Bicknell, G. V., Lovell, J. E. J., et al. 2012, ApJ, 755, 174

Godfrey, L. E. H., Lovell, J. E. J., Burke-Spolaor, S., et al. 2012, ApJ, 758, L27

Goodger, J. L., Hardcastle, M. J., Croston, J. H., et al. 2010, ApJ, 708, 675

Hardcastle, M. J. 2006, MNRAS, 366, 1465

Hardcastle, M. J., Kraft, R. P., Sivakoff, G. R., et al. 2007, ApJ, 670, L81

Hardcastle, M. J., Massaro, F., Harris, D. E., et al. 2012, MNRAS, 424, 1774

Harris, D. E., & Krawczynski, H. 2006, ARA&A, 44, 463

Harris, D. E., Cheung, C. C., Stawarz, Ł., Biretta, J. A., & Perlman, E. S. 2009, ApJ, 699, 305

Harwood, J. J., & Hardcastle, M. J. 2012, MNRAS, 423, 1368

Hogan, B. S., Lister, M. L., Kharb, P., Marshall, H. L., & Cooper, N. J. 2011, ApJ, 730, 92

Jester, S., Harris, D. E., Marshall, H. L., & Meisenheimer, K. 2006, ApJ, 648, 900

Kataoka, J., Stawarz, Ł., Harris, D. E., et al. 2008, ApJ, 685, 839

Marshall, H. L., Miller, B. P., Davis, D. S., et al. 2002, ApJ, 564, 683

Marshall, H. L., Hardcastle, M. J., Birkinshaw, M., et al. 2010, ApJ, 714, L213

Marshall, H. L., Gelbord, J. M., Schwartz, D. A., et al. 2011, ApJS, 193, 15

Massaro, F., Harris, D. E., & Cheung, C. C. 2011, ApJS, 197, 24

Million, E. T., Werner, N., Simionescu, A., et al. 2010, MNRAS, 407, 2046

Mingo, B., Hardcastle, M. J., Croston, J. H., et al. 2011, ApJ, 731, 21

Perlman, E. S., Biretta, J. A., Sparks, W. B., Macchetto, F. D., & Leahy, J. P. 2001, ApJ, 551, 206

Pudritz, R. E., Hardcastle, M. J., & Gabuzda, D. C. 2012, Space Sci. Rev., 169, 27

Sambruna, R. M., Gambill, J. K., Maraschi, L., et al. 2004, ApJ, 608, 698

Schreier, E. J., Feigelson, E., Delvaille, J., et al. 1979, ApJ, 234, L39

Schreier, E. J., Gorenstein, P., & Feigelson, E. D. 1982, ApJ, 261, 42

Schwartz, D. A., Marshall, H. L., Lovell, J. E. J., et al. 2000, ApJ, 540, L69

Schwartz, D. A. 2002, ApJ, 569, L23

Siemiginowska, A., Smith, R. K., Aldcroft, T. L., et al. 2003, ApJ, 598, L15

Siemiginowska, A., Stawarz, Ł., Cheung, C. C., et al. 2007, ApJ, 657, 145

Siemiginowska, A., Stawarz, Ł., Cheung, C. C., et al. 2012, ApJ, 750, 124

Sobolewska, M. A., Siemiginowska, A., Migliori, G., et al. 2012, ApJ, 758, 90

Tavecchio, F., Maraschi, L., Sambruna, R. M., & Urry, C. M., 2000, ApJL, 544, L23

Willingale, R. 1981, MNRAS, 194, 359

Wang, J., Fabbiano, G., Elvis, M., et al. 2011, ApJ, 736, 62

Worrall, D. M. 2009, A&A Rev., 17, 1

Project Scientist's Report

Martin Weisskopf

Wow! *Chandra* is now well into its 15th year of operation with every expectation of continuing into the foreseeable future. This Fall (tentatively November 17-21), we shall celebrate 15 Years of *Chandra* Science at a symposium in Boston.

With no new major X-ray-astronomy facility planned to launch before 2028 (ESA's L2 mission), the entire *Chandra* Team recognizes the importance of maintaining *Chandra*'s unique science capabilities for at least another decade. As the Observatory ages, three issues—thermal, contamination, and radiation—are resulting in graceful degradation of the science performance.

Continued breakdown of the thermal insulation makes efficient science operation progressively more challenging, as thermal issues further constrain operations. Growing molecular contamination on the ACIS slowly erodes the net efficiency at low energies. Radiation damage to ACIS results in increasing charge-transfer inefficiency, but at a rate that is now manageable. Project Science (PS) has been particularly engaged in addressing the latter two (ACIS-specific) issues—molecular contamination and radiation damage. PS leads molecular-transport modeling for the ACIS cavity, with the goal of understanding the observed accumulation and then investigating potential scenarios for reduction. Over the past year, PS has also spearheaded efforts to ensure continued availability of real-time space-weather data on the low-energy protons that damage the ACIS front-illuminated CCDs.

With Harvey Tananbaum, Belinda Wilkes, Wallace Tucker, and Peter Edmonds of the CXC, we have prepared a major review article, "Highlights and Discoveries from the *Chandra* X-ray Observatory" to appear in the journal Reports on Progress in Physics. Also with the CXC, the *Chandra* Project—including Project Science—is preparing for (*Chandra*'s 4th) biennial Senior Review of Operating Missions, scheduled for 2014 March.

Finally, I would like to acknowledge the extraordinary contributions Harvey Tananbaum has made to the success of the *Chandra* mission during his time as CXC Director. For 37 years, I have worked with Harvey to create and now to operate this Great Observatory. In this day of smartphones and contact lists, his is the only phone number that I can call without invoking

the voice assistant on my iPhone. Harvey's stepping down as CXC Director will mark the end of an era in *Chandra*'s history. Everyone associated with *Chandra* owes him a deep debt of gratitude.

Project Manager's Report

Roger Brissenden

Chandra marked over fourteen years of successful mission operations with continued excellent operational and scientific performance. Telescope time remained in high demand, with significant oversubscription in the Cycle 15 peer review, held in June. The Cycle 15 review approved 179 proposals out of 636 submitted by researchers worldwide who requested 106 Msec of observing time, $\sim$ 5.3 times greater than the time available. Among the approved proposals are two X-ray Visionary Projects (XVPs), which were allocated a total of 5 Msec. XVPs are longer observing programs intended to address major questions in astrophysics and to produce data sets of lasting value.

In the Fall of 2013, the observing program transitioned from Cycle 14 to Cycle 15. Due to the gradual evolution of *Chandra*'s orbit, which has reduced the nonproductive time spent in Earth's radiation belts, *Chandra*'s overall observing efficiency has risen to the highest level of the mission. As a result, observing cycles 13–15 have benefitted from a significant increase in available observing time, but the orbit is now evolving back toward less time above the belts. We released the Call for Proposals for Cycle 16 in December, and look forward to the Cycle 16 peer review in June 2014.

In response to NASA's request for proposals for the 2014 Senior Review of operating missions, *Chandra* X-ray Center (CXC) and Marshall Space Flight Center program staff are at the time of this writing preparing the *Chandra* proposal, due in January 2014 and to be followed by a site visit to the CXC by the review committee in March 2014.

In October the CXC hosted the annual symposium for the Einstein Fellowship program. A CXC workshop, "The X-ray View of Galaxy Ecosystems," originally planned for the summer of 2013, was canceled due to NASA restrictions on conferences and travel resulting from congressional sequestration of funds. CXC has rescheduled the workshop for the summer of 2014. As part of the CXC's regular reviews and consultations with outside organizations, NASA reviewed the CXC's operations in April and November, and the *Chandra* Users' Committee met at the CXC in October.

After several years of very low solar radiation, the sun has become more active, requiring the team to interrupt *Chandra* observing 4 times during the year to protect the instruments from solar particles. In addition, eight requests to observe targets of opportunity required the mission planning and flight teams to interrupt and revise on-board command loads. *Chandra* passed through the 2013 spring and fall eclipse seasons with nominal power and thermal performance.

CXC staff completed a study of the Fine Sun Sensors (FSS), which are used to orient the spacecraft during certain non-observing conditions and safe modes. In 2012 the active sensor, FSS-A, began producing erroneous readings near the edge of its field of view (FOV), believed due to reflection of light from nearby thermal insulation. The study showed that the alternate sun sensor, FSS-B, operates properly, and that FSS-A is fully functional for safe modes, which do not require operation near the edge of the FOV. In May 2013 the team swapped primary operation to FSS-B, with FSS-A held in reserve for safe modes. The system is fully functional for both normal and safe mode operations.

In early 2013, one of the four thrusters used for unloading angular momentum showed decreased thrust. The thruster continues to be useable, but its remaining life appears limited. A check-out of the redundant, B-side, thruster set showed that one of its four thrusters was inoperative, likely due to a failed electrical connection. Following a careful assessment, the team swapped the system to the B side for normal operations, with the failed B-side thruster not used and the A-side thrusters reserved for safing. With the new thruster configuration, *Chandra* can properly manage momentum for normal operations and retains full safing capability.

Chandra's focal plane instruments, the Advanced CCD Imaging Spectrometer and the High Resolution Camera, have continued to operate well and have had no significant problems. ACIS, along with the overall spacecraft, has continued to warm gradually due to slow degradation of the spacecraft's multi-layer thermal insulation. All systems at the *Chandra* Operations Control Center continued to perform well in supporting flight operations. *Chandra* data processing proceeded smoothly and data distribution continued to be rapid, with the time from observation to receipt by the observer averaging $\sim$ 30 hours.

The CXC's Data System team released software to support *Chandra* users with Cycle 15 observation proposal submissions, the Cycle 15 Peer Review, and the Cycle 16 Call for Proposals. In addition, in June the team released a major upgrade to the data system that migrates the *Chandra* Data System's data processing software from Solaris to 64-bit Linux. The *Chandra* Source Catalog (CSC) currently includes about 107,000 individual sources. The CXC is in the process of developing a major new release, expected to triple its size, that will co-add multiple observations and use new source detection and background algorithms to include the faintest (~ 5 net counts) sources.

The CXC Communications and Public Engagement (CPE) group created 12 science press releases, 1 non-science press release and 25 image releases resulting in 2891 articles in print and electronic news outlets. *Chandra* images were used in 15 instances as the HEASARC Picture of the Week, 3 Astronomy Picture of the Day, and 3 NASA Picture of the Week. The group produced 30 podcasts on *Chandra* results as well as special series for children and on fundamental science topics related to astrophysics. In addition, 40 blog entries were posted, including additions to "Meet the Astronomer" profiles with PI's of *Chandra* science results and "Women in the High Energy Universe" to focus attention on women's careers in astronomy.

Although participation in education and outreach activities was constrained by sequestration restrictions, the CPE team presented 23 workshops at conferences and clinics sponsored by the National Science Teacher Association and the National Science Olympiad. The "Here, There, and Everywhere" traveling exhibit continued its national tour of one site per month at small libraries and museums. The training video to support Science Olympiad Coaches was updated. The *Chandra* 3D model of Cas A was chosen as one of the initial offerings of the Smithsonian Digitization initiative and was produced as a hardcopy model through 3D printing. An interactive skymap of *Chandra* sources was released and all *Chandra* images are now available through the Astropix feed. No new printed materials were produced because of sequestration constraints but *Chandra* was able to fill 396 requests for over 28,000 items of educational materials out of existing inventory. A new electronic product line of "infographics" was produced for download from the *Chandra* web site.

We look forward to a new year of continued smooth operations and exciting science results.

A Message of Thanks to Harvey Tananbaum, Founding Director of the CXC

The *Chandra* Team

As previously announced, Dr. Harvey Tananbaum will soon be stepping down as Director of the *Chandra* X-ray Center. Harvey has been the Director since the formation of the CXC in 1991 and his contributions to the success of *Chandra* through this role and as a driving force in the development of the mission (originally AXAF) have been extraordinary.

From AXAF's original design, conceived by Riccardo Giacconi, Harvey was instrumental in guiding the maturing concept through the many proposal and review cycles to the final approval by NASA as a mission. Already a distinguished scientist, he also became an expert politician and advocate in the process, leading the team as it navigated the numerous budget re-plans, re-designs, and modifications required to reach final approval.

Along the path to launch, Harvey led the Mission Support Team that provided key science, calibration and technical support to NASA as *Chandra* was developed. He led the successful proposal for the *Chandra* X-ray Center to be located at the Smithsonian Astrophysical Observatory, and he built the dedicated team that has operated *Chandra* and served the science community for almost 15 years.

Without Harvey's skilled, dedicated, exacting and inspiring leadership *Chandra* and the CXC/MSFC/MIT/GTO/Northrop-Grumman team would not be as strong and successful as it is today. Harvey watches over every aspect of *Chandra* – even when (appearing to be) dozing during meetings! He pushes us to take one, two, three (or more!) extra step(s) in everything we do: to improve on a calibration product or a webpage, move up a release date, observe a TOO earlier, extend one more helping hand to an observer, provide one more, accurate statistic, take the analysis of an instrument or spacecraft problem one stage deeper – all motivated by maximizing the scientific output of *Chandra*, protecting the observatory, and serving our community to the best of our abilities. Harvey's exemplary leadership combined with the excitement of the *Chandra* mission and science has resulted in a strong, loyal, dedicated, and committed team which will continue to work hard for many years to ensure *Chandra*'s legacy.

To mark Harvey stepping down as our "fearless leader," we the members of the extended *Chandra* team would like to express our heartfelt thanks for all the years that you have worked to make *Chandra* a success, for your inspirational leadership, your unswerving dedication to our mission, and your enduring support to each and every one of us, past and present. It has been a privilege to work for you and our team will not be the same without you at the head, but your legacy will ensure our continued success.

Belinda Wilkes Appointed as Director of the CXC

In consultation with NASA, CfA Director Charles Alcock has appointed Belinda Wilkes to succeed Harvey Tananbaum as the director of the *Chandra* X-ray Center. Charles notes that Belinda "has demonstrated the expertise necessary to lead the CXC and to continue and extend the success of the *Chandra* mission." She assumes the directorship on April 20, 2014.

Belinda has served as the CXC Assistant Director for the past 12 years. She is well known to *Chandra*'s international user community particularly through her leadership of the annual *Chandra* Peer Review. Belinda maintains strong and effective working relationships at the CXC, with NASA Headquarters and the Marshall Space Flight Center (MSFC), which manages *Chandra*.

Jeffrey Hayes, *Chandra* Program Executive in NASA's Science Mission Directorate said, "I have known and worked with Belinda Wilkes for a number of years. I am so very pleased to know that the *Chandra* mission will be continuing under such capable hands."

Martin Weisskopf, *Chandra*'s Chief Scientist commented: "Belinda Wilkes will be an outstanding Director and will continue the tradition of advancing astronomy and astrophysics via *Chandra*'s unique and vital contributions to these fields."

Jon Miller, University of Michigan, Ann Arbor, Chair of the *Chandra* Users' Committee said, "Belinda Wilkes is a first-rate scientist who really connects with the ever-expanding community of *Chandra* users. It is terrific that she will be guiding *Chandra* into the future."

The *Chandra* Team welcomes Belinda enthusiastically to her new role as Director. Belinda, we look forward to working together to support many more years of spectacular *Chandra* science!

Of Programs and Papers: Making the *Chandra* Connection

Sherry Winkelman and Arnold Rots

Proposal/Grant/Paper Linking Process

The *Chandra* bibliography is a complicated database storing metadata about publications closely connected in some way to the *Chandra* mission. It includes all publications related to the *Chandra* mission, from *Chandra* science papers to publications about the instruments, software, and operations of the CXC. In the last year we have expanded the bibliography to include metadata describing, among other things: the general content of papers; justifications for inclusion in the bibliography; where/how *Chandra* data links are made to papers; and *Chandra* related details about acknowledgments and grants included in publications. These metadata are incomplete and will take time to be fully populated, but when finished, the *Chandra* bibliography will be a much richer resource for scientific, bibliographic, and historical investigations.

Our initial focus is to populate metadata related to *Chandra* theory and archive grant acknowledgments, since that is the only mechanism that allows us to track such publications related to those programs except perhaps for dataset IDs in the archival case. We have completed an ADS full-text search for all grants from *Chandra* cycles 1-14 against all searchable papers in ADS as of June 27, 2013. For each archive and theory grant reference, we have determined whether the paper is related to the abstract of the proposal linked to the grant, and to which institution the grant was attributed.

Maintaining the *Chandra* Bibliography

The CDA relies heavily on ADS for locating potential *Chandra*-related publications and we have automated as much of the process as possible to reduce the number of papers we examine that are unrelated to *Chandra*. We query ADS once a week for all papers which have "chandra," "axaf" or "x-ray" in the title, abstract or keywords, adding new bibcodes to our working database. We average 100 new bibcodes per week. We then download each of those papers, convert them to text, and flag for manual inspection those papers containing the word 'chandra'. At this point we have 40 new bibcodes a week to classify, 45%

of which are *Chandra* science papers as defined at http://cxc.harvard.edu/cda/bibstats/bibstats.html.

In the next few months we will collect new bibcodes weekly by using the full-text search interface from ADS to scan *Chandra* grants acknowledged in publications. We expect this to yield about 5 bibcodes more per week to classify. We would like to eventually expand our initial search against ADS to include all astronomy papers. Until we have some semantic search capabilities able to focus on *Chandra* science papers, this may increase our classification load significantly while only adding a few percent to the *Chandra* science paper category, so is therefore not currently cost-effective.

Recommendations to Authors

There are several things that you as PIs and authors can do to make grant acknowledgments meaningful and a useful resource to the *Chandra* bibliography: (1) acknowledge your grant as coming from *Chandra*; (2) check that the grant number is correct; and (3) only acknowledge your *Chandra* grant if the work presented in the paper is related to the proposal that the grant comes from. We also encourage authors to use dataset identifiers in their AAS manuscripts as a means of creating direct links to the data used in their publications. You can find details on using and/or creating dataset identifiers at the CDA website, http://cxc.harvard.edu/cda/datasetid.html.

Chandra Related Meetings and Important Dates

Cycle 16 Peer Review: June 23–27, 2014

Cycle 16 Cost Proposals Due: September 17, 2014

X-ray Galaxy Workshop: July 9-11, 2014

Users' Committee Meeting: October, 2014

Einstein Fellows Symposium: Fall 2014

Cycle 16 Start: December, 2014

Cycle 17 Call for Proposals: December, 2014

ACIS Update

Paul Plucinsky, Royce Buehler, Gregg Germain, & Richard Edgar

The ACIS instrument continued to perform well over the past year while conducting the vast majority of GO observations with *Chandra*. There were only minor anomalies that affected the quality of the science data for a few observations. The charge-transfer inefficiency (CTI) of the FI and BI CCDs is increasing at the expected rate. The contamination layer continues to accumulate on the ACIS optical-blocking filter (see article herein by Larry David). A new calibration file to model the absorption due to the contamination layer was released by the CXC calibration group in the 4.5.9 release of the *Chandra* Calibration Database (CALDB) on 19 November 2013. This calibration file significantly improves the accuracy of the model for data acquired after mid-2012. If GOs are analyzing data acquired from mid-2012 or later and the response at low energies is important for their analysis, they should be using the contamination model in CALDB 4.5.9 or later.

The ACIS flight software team developed a patch in 2011 that allows ACIS to recognize sharply increasing count rates on all active CCDs as a signature of the onset of a radiation storm. This patch was developed in response to the continued degradation in sensitivity of the EPHIN instrument to high radiation as the operating temperature of EPHIN increases. ACIS now produces a high radiation signal to the *Chandra* onboard computer (OBC) and the OBC acts upon this trigger (as of May 2012) by sending the necessary commands to protect the science instruments (SIs). The HRC anti-coincidence signal is also used by the OBC as a radiation monitor. Since the ACIS radiation monitor patch has been implemented, there have been two occurrences (both in 2013) in which the high radiation signal was produced by ACIS and the SIs were safed by the OBC without any false triggers. The probability of a false trigger from EPHIN has been increasing as the temperature continues to increase. After observing successful SI safing based on both the ACIS and HRC radiation triggers, the *Chandra* Flight Operations Team has removed the EPHIN radiation signal from the OBC safing logic.

Control of the ACIS focal plane (FP) temperature continues to be a major focus of the ACIS Operations Team. As the *Chandra* thermal environment contin-

ues to evolve over the mission, some of the components in the Science Instrument Module (SIM) close to ACIS have been reaching higher temperatures, making it more difficult to maintain the desired operating temperature of -119.7 °C at the focal plane. GOs can increase the probability that the FP temperature will be cold and stable for their observation by reducing the number of operational CCDs, which reduces the power dissipation in the FP, thereby resulting in a lower FP temperature. GOs can select CCDs as "required" or "optional" for their observation. Starting in Cycle 16, GOs will be encouraged to select a maximum of 4 required CCDs for their observations to keep the FP and the electronics cooler, if their science objectives can be met with 4 or fewer CCDs. GOs are still allowed to select 5 CCDs as required when they submit their proposals. Starting in Cycle 14, GOs were not allowed to select "Y" for 6 CCDs in the RPS forms when they submit their proposal. If a GO requires 6 CCDs for their observation, they are to select 5 CCDs as "Y" and one CCD as "OFF1" at the time of proposal submission. If the proposal is selected, the GO may work with their User Uplink Support Scientist and change the "OFF1" to a "Y" if the sixth CCD is required. However, GOs should be aware that requesting 6 CCDs increases the likelihood of a warm FP temperature and/or may increase the complexity of scheduling the observation. GOs should review the updated material on selecting CCDs for their observations in the Proposers' Guide and on this web page: http://cxc.harvard.edu/acis/optional_CCDs/optional_CCDs.html.

The control of the ACIS electronics temperatures continues to be a concern for the ACIS Operations Team. ACIS has three main electronics boxes, the Power Supply and Mechanisms Controller (PSMC), the Digital Processing Assembly (DPA), and the Detector Electronics Assembly (DEA). The PSMC reaches its highest temperatures when the satellite is in a "forward Sun" configuration—pitch angles between 45-60 degrees (*Chandra* cannot point within 45 degrees of the Sun), and the DPA and DEA reach their highest temperatures when the satellite is in a "tail-Sun" orientation—pitch angles between 130-160 degrees. The *Chandra* FOT uses the optional CCDs information provided by GOs to turn off optional CCDs if thermal conditions require. The recommendation in the previous paragraph to select only 4 required CCDs if the science objectives can be met with 4 CCDs, will also reduce the temperature of the PSMC, DEA, and

DPA in addition to the temperature of the FP. Given the benefit to the ACIS FP temperature and electronics temperatures, the CXC encourages GOs to select 4 or fewer required CCDs and select any additional CCDs as optional.

The High Resolution Camera

Ralph Kraft, Hans Moritz Guenther (SAO), and Wolfgang Pietsch (MPE)

It has been another quiet, but successful year for HRC operations. The instrument performs well with no significant anomalies or instrumental issues. The HRC continues to be used for a wide variety of astrophysical investigations. In this chapter, we briefly describe two such science studies. First, a collaboration led by Dr. Wolfgang Pietsch of MPE used the HRC to study the X-ray state of the nova population in M31 in conjunction with *XMM-Newton* and optical studies. They found that there is a strong correlation between the optical and X-ray properties of these novae. Second, Guenther et al. (2012) used the HRC-I to measure the X-ray flux from the nearby star β Pic. Combining the sensitivity of the HRC-I below 0.5 keV with an *XMM-Newton* detection, they demonstrated that the emission originates in the stellar corona, not the dusty disk, and that the temperature of the gas is ∼ 1.2 MK, making it the hottest low-mass stellar coronal source known.

The *Chandra* HRC detector was used in a joint program with the *XMM-Newton* observatory to study the supersoft X-ray state of optical novae in our neighbor galaxy M31. X-ray studies of novae are vital to gain a direct access to the physics of the underlying white dwarf that hosts the nova event. In six dedicated monitoring seasons from June 2006 to June 2012 (41 total HRC observations with integrated exposure of 750 ks), we discovered the supersoft X-ray counterparts of 38 novae and thereby doubled the number of such sources known in M31. The *Chandra* HRC with its excellent spatial resolution, large field of view and response at X-ray energies below 0.5 keV was crucial for detecting nova counterparts in the crowded central region of M31, where other X-ray observatories suffer from source confusion. A statistical analysis of the overall sample of 79 X-ray-detected novae in M31 revealed strong correlations between the optical and X-ray parameters of novae, showing essentially that novae that

decline rapidly in the optical are hot in X-rays, with short X-ray phases (Henze et al. 2010, 2011, 2013, see Fig. 1). In addition to the statistical analysis of the nova sample, several individual novae could be investigated in detail (e.g. novae in globular clusters and novae showing time variability).

To create a source catalog of the M31 center and search for time variability of the sources, we included 23 observations from November 1999 to February 2005 (adding about 250 ks exposure time). We detected 318 X-ray sources and created long term light curves for all of them. We classified sources as highly variable or outbursting (with subclasses short vs. long outbursts and activity periods). 129 sources could be classified as X-ray binaries due to their position in globular clusters or their strong time variability (see Fig. 2). We detected seven supernova remnants, one of which is a new candidate, and also resolved the first X-rays from a known radio supernova remnant (see Hofmann et al. 2013).

In a second study, Guenther et al. used the HRC to determine the origin of the X-ray emission from β Pic, a nearby star with a dusty disk. On the main sequence, there are two different mechanisms that generate stellar

X-ray emission. Massive O and B stars have radiatively driven winds, and because these winds are unstable, X-ray emitting shocks form. On the other end to the main sequence are the cool stars that produce X-ray emission in a magnetically heated corona like our sun. Stars of spectral type A lie between these regimes and should be X-ray dark. Yet, some of them have been detected in X-ray observations. One of the most peculiar of those objects is β Pic, an A5 star at only 19.5 pc. A previous 70 ks *XMM-Newton* observation (Hempel et al. 2005) barely detected β Pic in a very narrow energy band just around the O VII band. β Pic also has a strong IR excess due a a massive debris disk surrounding the star, made up from dust and cometary bodies. There are at least three scenarios for the origin of this X-ray emission: (i) a stellar corona, (ii) a boundary layer where mass is accreted from the disk or (iii) charge-exchange between the stellar wind and the comas of many comets.

A grating spectrum would easily select between these models, but alas, β Pic is much too faint. So, how do we get any spectral information for a star that is detected with just a dozen photons in more than 70 ks of
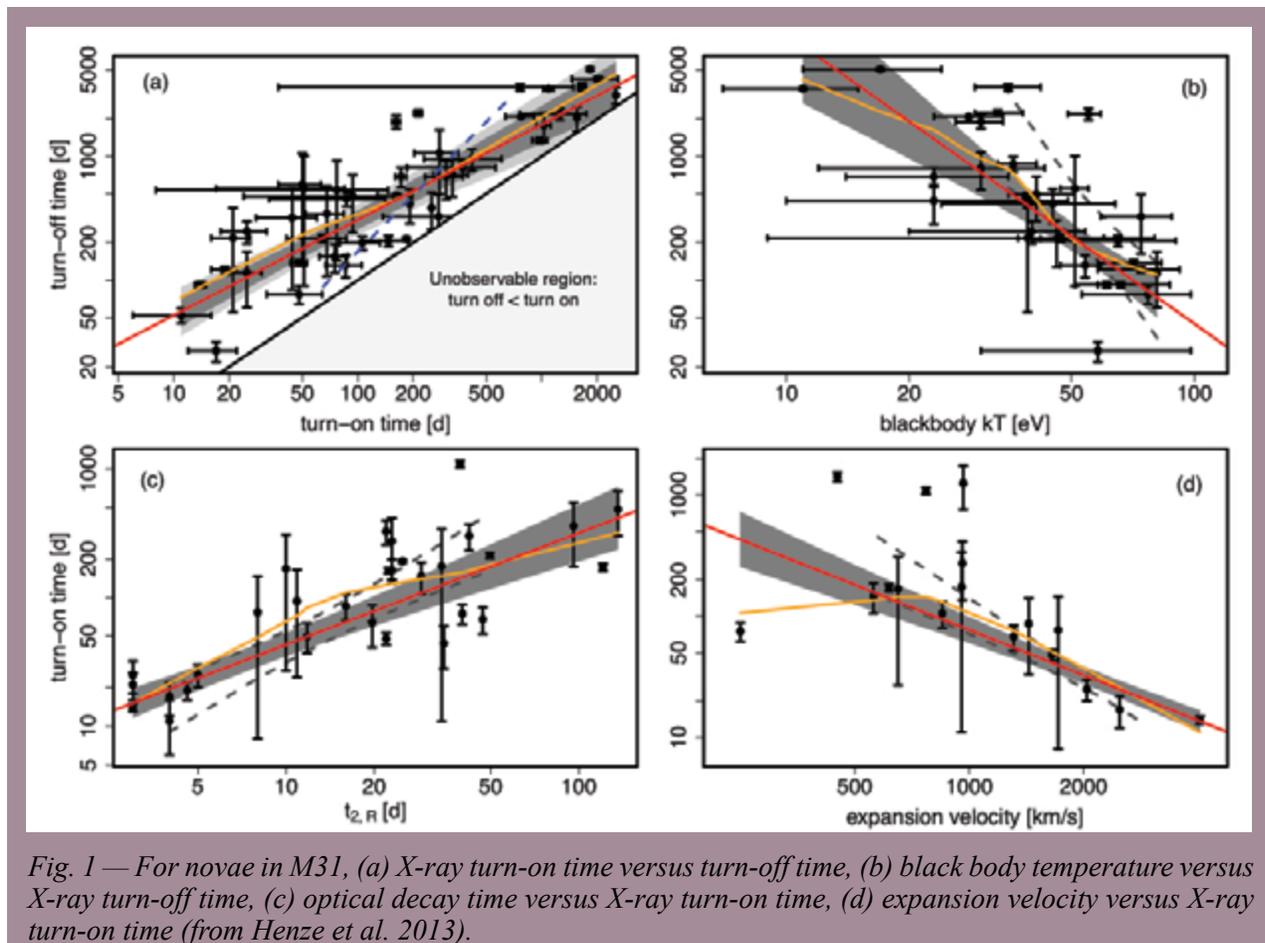

Fig. 1 — For novae in M31, (a) X-ray turn-on time versus turn-off time, (b) black body temperature versus X-ray turn-off time, (c) optical decay time versus X-ray turn-on time, (d) expansion velocity versus X-ray turn-on time (from Henze et al. 2013).

XMM-Newton? The answer is to go to a different band; scenario (ii) and (iii) should yield significant soft X-ray emission in the HRC bandpass, unique to *Chandra*. So, we observed β Pic for 20 ks with the HRC-I. In scenarios (ii) and (iii) there should have been hundreds of counts in the HRC-I, but we only saw 17 (see Fig. 3). From the ratio of count rates in the *XMM-Newton* observation and our new *Chandra*/HRC data, we conclude that β Pic has a 1.2 MK corona, and this X-ray emission is unrelated to its dust disk. Instead, this makes β Pic the hottest cool star, i.e. the hottest known star with magnetic activity.

References

Guenther et al. 2012, ApJ, 750, 78

Hempel et al. 2005, A&A, 420, 707

Henze et al. 2010, A&A 523, A89

Henze et al. 2011, A&A 533, A52

Henze et al. 2013, A&A in print arXiv: 1312.1241

Hofmann et al. 2013, A&A 555, A65

Fig. 3 — HRC-I image of β Pic, spatially binned by a factor of two. The shade indicates the number of counts per bin from light gray (1 count) to black (4 counts). The circle marks the extraction region centered on the optical position of β Pic (Guenther et al. 2012).
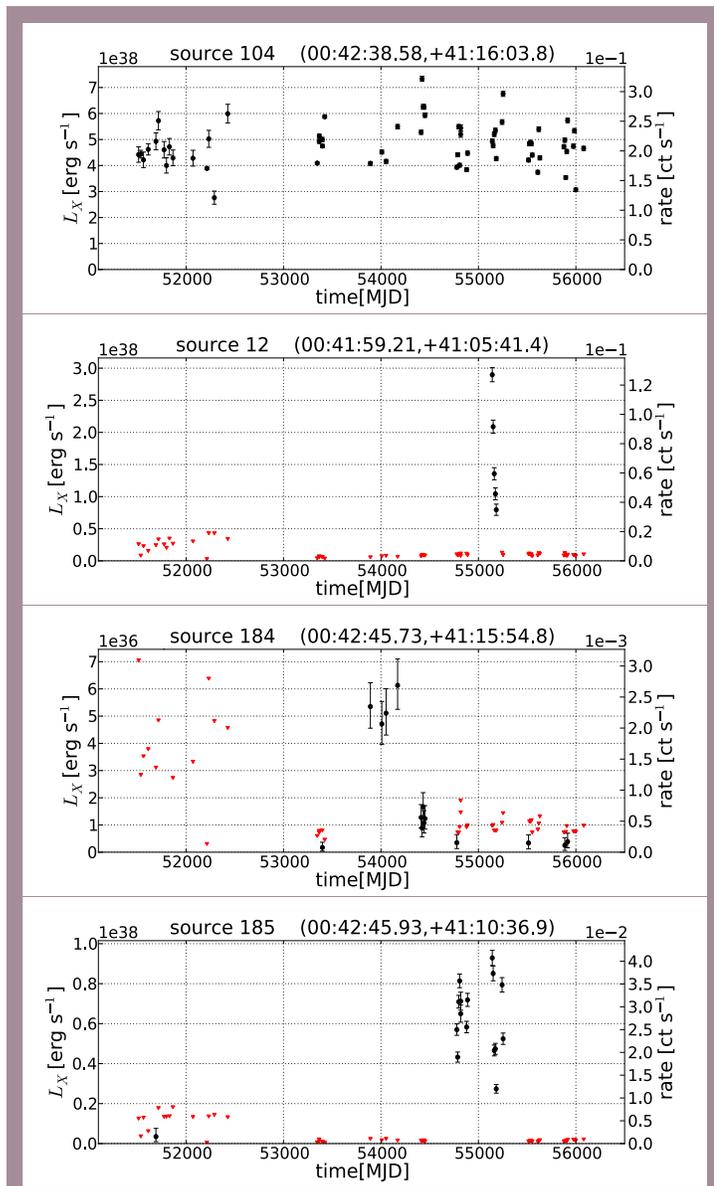

Fig. 2 — X-ray luminosity and photon count rate over modified Julian date: highly variable (source 104), short outburst (12), long outburst(184), activity period during outburst (185) (from Hofmann et al. 2013).
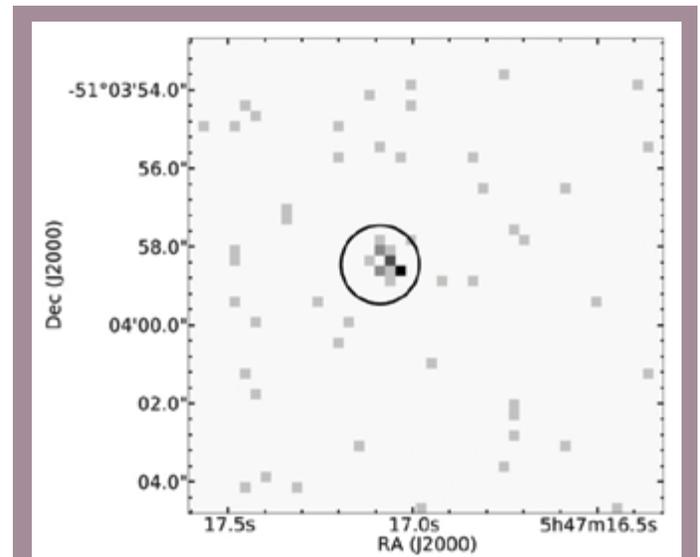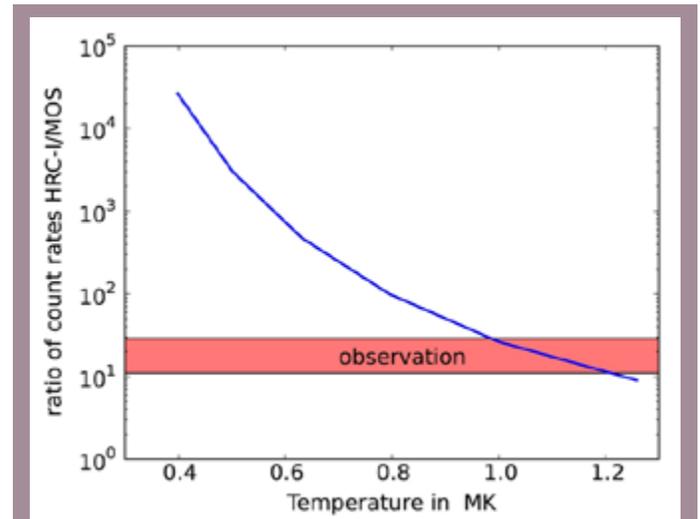

Fig. 4 — Ratio of HRC-I counts (full band) and MOS counts (O VII) as a function of plasma temperature for an optically thin, collisionally excited thermal plasma with solar abundances (Guenther et al. 2012).

HETG

David Huenemoerder (for the HETG team)

Performance, Calibration, and Software

In Cycle 14 there were 13 HETG programs comprised of exposures ranging from 15 ks to 656 ks, for a total of 2689 ks.

There were no major calibration updates in the past year. The CXC Calibration Group continues to monitor and update the ACIS contamination model as necessary, the grating spectra being key in this regard. A major effort to understand the continuous-clocking (CC) mode response has been completed. Good news: there is no significantly different response of the CCDs in CC-mode. Bad news: certain anomalies are due to source science and will require some effort on the analyst's part to disentangle them. The fundamental issue is that many of the very bright sources observed in CC-mode have large, bright, and soft dust-scattering haloes. When these are dispersed and then collapsed to a one-dimensional spectrum, they produce a "background" under the point-source's spectrum, with a complicated spatial-spectral morphology which will weaken and blur absorption edges. This is explained in detail in http://cxc.harvard.edu/cal/projects/index.html.

In CIAO 4.6, a new grating tool was released, `tgdetect2`, which completes the source detection improvements for CIAO reported here last year. The new tool uses empirical source rate statistics to determine whether to run the bright-source detection mode appropriate for distorted (or absent) zeroth orders (`tg_find-zo`, which finds the CCD frame-shift streak and grating spectrum intersec-

tion), or the faint-source program (`tgdetect`) thus saving the user having to know which method to use.

Several enhancements to the *Chandra* grating spectral catalog, TGCat[1] were implemented. Source searches by name are now more forgiving, return-

---

1 http://tgcat.mit.edu/
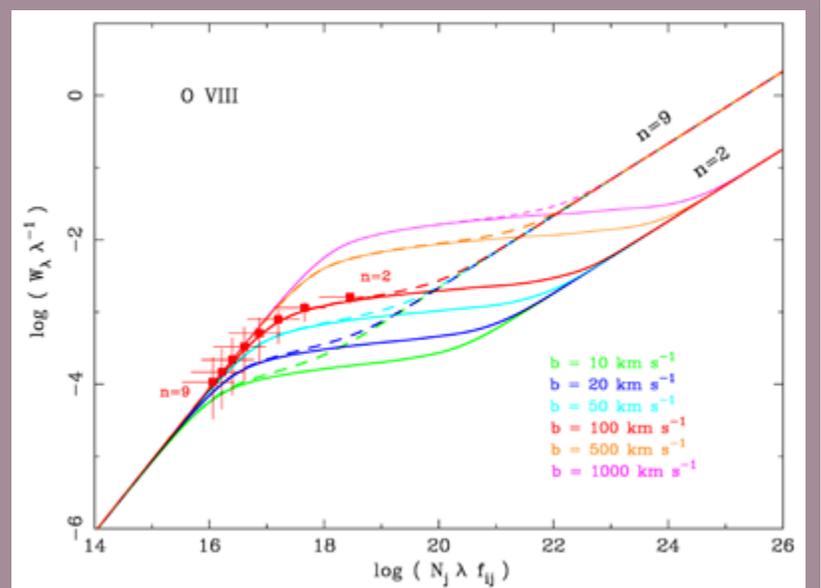
Fig.1 — The curve of growth in O VIII in IRAS 13349+2438 from a simultaneous fit to the the absorption lines in the HETG spectrum from upper levels n = *2 to 9. With only the first two lines in the series, there would be an order-of-magnitude uncertainty in the column density. (From Lee et al. 2013).*

Fig. 2 — SS 433 spectrum (black) from 1.5–4.5 Å (top) and 3.0–6.5 Å (bottom). Red is the scaled and broadened θ¹Ori C spectrum, and green a scaled, unbroadened version. (From Marshall et al. 2013.)

ing close matches if an exact sub-string match is not found. In the interactive plotter, you can now save the parameters and apply them to one or more plots, you can generate multiple plots for a selection of multiple extractions, and you can mark the positions of major spectral features. TGCat users who find a serendipitous spectrum i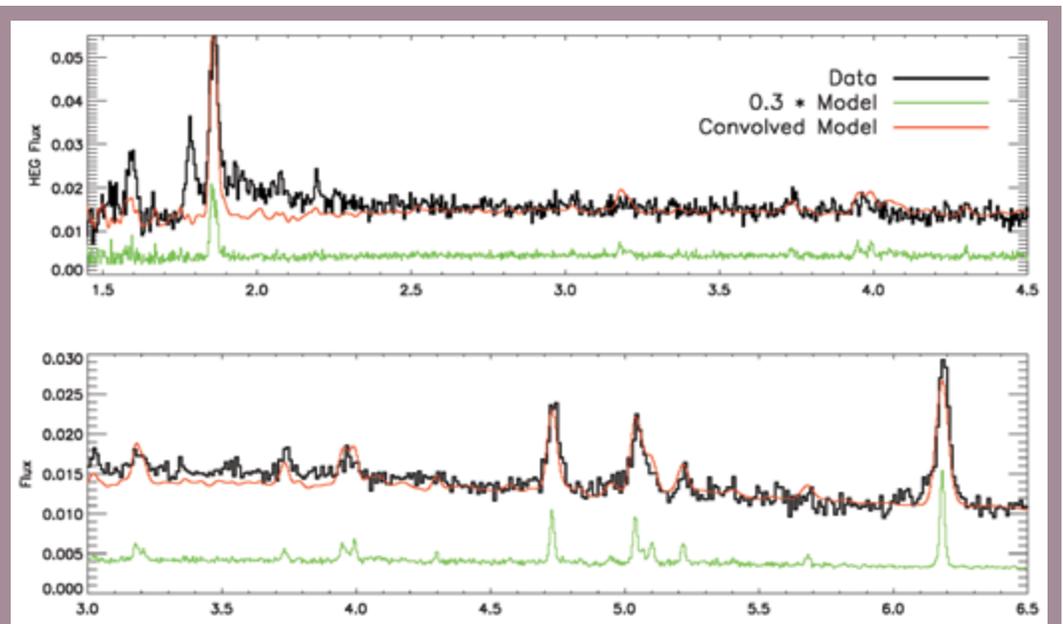n an image can send in a request for processing using a form on the main page, and the result will be run and posted to the catalog within a day or two.

Selected Scientific Highlights

About a dozen papers using HETG data went into press in the past year, many using archival data, and some using observations going back to *Chandra*'s first cycle, a testament to the value of the archive and the richness of the data. While we know that astronomical objects are not comprised of spherical homogeneous plasmas, we often have difficulty resolving detailed structure. Several of the works in the past year have made use of the high-resolution of HETG (in conjunction with spatial and temporal resolution) to probe the source geometry.

A Quasar

Lee et al. (2013 MNRAS 430, 2650) undertook a large, multi-band coordinated attack on the quasar IRAS 13349+2438, from the infrared to X-rays. With spectra, they probed the outflow: all X-ray absorption lines were blue-shifted, and by similar amounts as in the UV emission lines. Their simultaneous fits to X-ray, H-, or He-like absorption line series clearly demonstrated their value in curve-of-growth analysis, providing data on the linear part of the curve which constrains measurement of the absorbing column to a much higher degree than can be done with the low-n transitions alone (see Fig. 1). From their comprehensive analysis, they were able to conclude that the X-ray-UV ionizing spectrum implies a continuous distribution of ionization states in a smooth flow rather than discrete clouds in pressure equilibrium as claimed previously.

A Micro-Quasar

> *They call it SS-433, and they found out it's-a coming toward Earth at 30,000 miles a second. But.. it's also going away from Earth at 30,000 miles a second. (1979, Father Guido Sarducci, a.k.a Don Novello[2])*

Zooming in from the extragalactic macro-quasar to a Galactic micro-quasar, SS 433, we have another

2 http://snltranscripts.jt.org/78/78rupdate.phtml

multi-band study by Marshall, et al. (2013 ApJ, 775, 75), comprised of contemporaneous radio to X-ray observations. The source is quite variable, both in flux (it is an eclipsing system) and—of course—in its signature Doppler shifts from the "it's-a coming and a going" jets. By summing spectra aligned on the blue-shifted jet, they found the spectrum to be thermal, not photoionized, and in fact empirically very similar to the broadened spectrum of θ^1 Ori C, a stellar wind-shocked thermal plasma (see Fig. 2). Given the
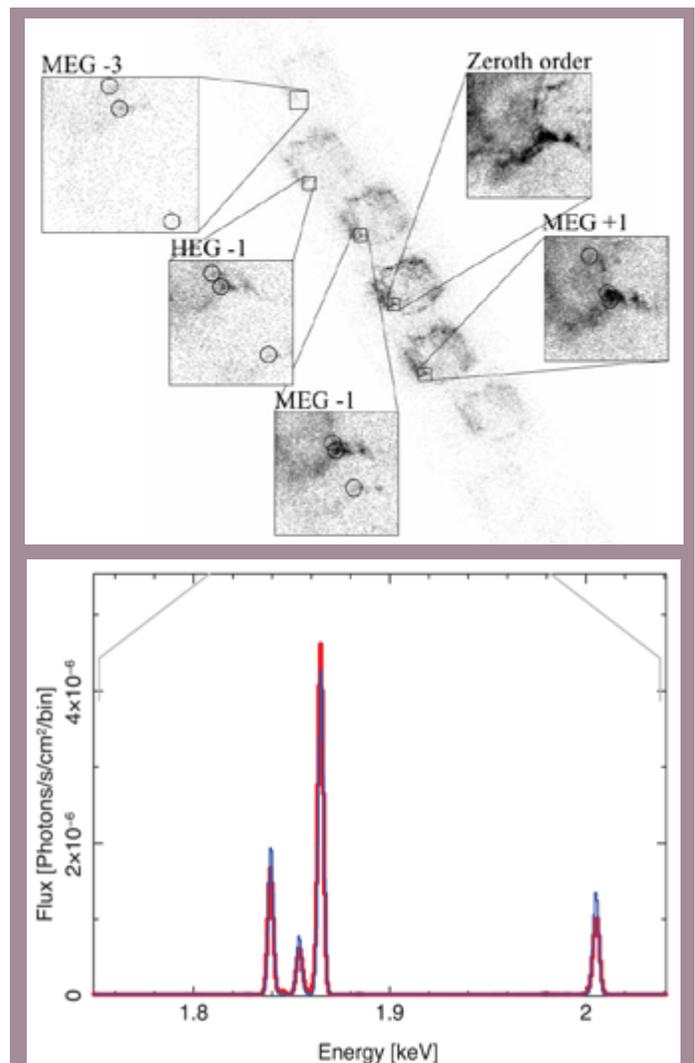
Fig. 3 — Cas A dispersed; top: diagonally on the left we see the -1, zeroth, and +1 orders, with a zoom in the labeled boxes to the right. Circles in the MEG+1 box show the positions of the H-like and He-like Si lines; these are shown in histogram form in the bottom panel, with nearly indistinguishable models and data in different colors. From left-to-right these are the forbidden, intercombination and resonance lines of the Si XIII triplet, and then the Si XIV H-Lyα-like line. (See the original publication for un-cropped figures; from Rutherford et al. 2013.)

thermal nature, the jet base density was determined from the spectrum to be about 10^{10}–10^{13} cm^{-3}. Abundances seem unusual (assuming typical or plausible supernovae progenitors for the compact object) with Ni enhanced by about a factor of 15. They found that the jet flow starts as a continuous plasma, then forms clumps.

A Micro-Blazar?

Vilhu and Hannikainen (2013 A&Ap, 550, A48) have suggested that Cyg X-3, a high-mass X-ray binary, is a "micro-blazar," since it is probable that its jet is directed nearly at Earth. Its jet shock, they hypothesize, enhances or creates clumps in the massive embedding wind of the companion Wolf-Rayet star. In their model, the jet paints a transient trail in the wind, and then the X-ray-binary can be observed through this disturbance, with a specific phase dependence. Their clumpy scenario gave a better fit to HETGS emission line variations than did a smooth model.

A Supernova Remnant

Rutherford et al. (2013 ApJ, 769, 64) have used a decade-long baseline of Cas A observations to study the kinematics and structure of this photogenic supernova remnant. In this work, they performed sophisticated spatial-spectral analysis of the dispersed image, fitting the two-dimensional distribution, to study individual knots in the remnant, achieving superb consistency between the high-resolution grating and ACIS imaging spectra. The grating spectra provided such useful diagnostics as resolved Si XIII triplets which were fit with non-equilibrium models (see Fig. 3). From the spectra and lack of significant variability over the past decade, they concluded that there are two distinct plasmas present, one high of metallicity, and one low metallicity, which are unmixed at small spatial scales.

It has been a good year for the High Energy Transmission Grating ("*where all the sources are strong, all the spectra are good looking, and all the results are above average*").

LETG

Jeremy Drake

Calibration Vortex

I write while blasted this winter by another encroachment of the cliched, nouveau-famed polar vortex that we are all completely fed up with hearing about from the media. This brings me to the LETGS calibration. It is a sort of vortex of iteration itself, though has of course nothing to do with the polar vortex. That goes aimlessly around and around in circles leaving people completely cold and gets joked about on late-night television, while the LETGS has never even been mentioned on late-night television. Yet.

The calibration vortex currently gripping the LETGS revolves around the chilling circular task of maintaining consistency with the slippery calibrations of the other *Chandra* instruments, all under the constraint that the absolute calibration based on hot white dwarfs should not thaw out. In *Chandra* Newsletter 20, I described a fairly successful operation to re-calibrate the HRC-S quantum efficiency following an increase in the detector high voltage. The voltage change was implemented to mitigate gain droop that had steadily sapped the quantum efficiency at an av-
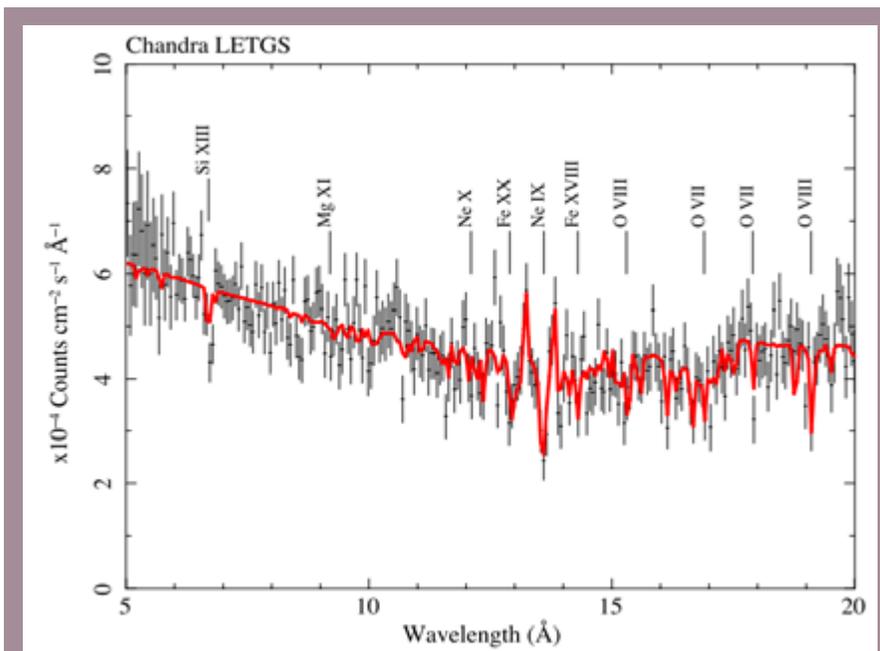

Fig. 1 — LETG+HRC-S spectrum of the Seyfert galaxy NGC 4593 in the 5–20 Å region, showing prominent absorption lines due to Si XIII, Ne IX and O VIII, as well as several other weaker features, that betray the warm absorber outflow. The absorption lines are formed within 30 pc from the central accretion vortex. From Ebrero et al. (2013).

erage rate of about 1.6% per year. We observed the hot—despite the polar vortex—white dwarf HZ43 and the still blazing blazar Mkn 421 at both new and old voltage settings to determine that the QE jumped back up by about 6% at the longest wavelengths covered by the instrument (100–170 Å) and about 4% or so at shorter wavelengths. This calibration was built into a subsequent CALDB release.

A perennial problem for the LETGS, however, is the lack of a bright absolute calibrator in the 30–60 Å range, where extragalactic sources tend to become too absorbed and uncertain in terms of spectral energy distribution, and hot white dwarfs like HZ43 lose signal to the precipitous downward slope of the Wien tail. We therefore returned to a slightly fainter old friend, RX J1856.5−3754. Touted as a possible quark star candidate, this intriguing isolated neutron star was observed extensively using the LETG under a 500 ks

Director's Discretionary program back in 2001. It has a blackbody-like spectrum with a temperature of about 60 keV (Burwitz et al. 2003; Drake et al. 2002). It rotates, just like a polar vortex except a bit quicker, every 7 seconds, modulating its X-ray emission on this period by about 1% (Tiengo & Mereghetti 2007). Monitoring over the years by *XMM-Newton* confirms the source is impervious to the polar vortex and remains essentially constant on the decade timescales we are concerned with (Sartore et al. 2012)—the key characteristic for a calibration monitoring source.

Recently, the MPE and SRON teams teamed up with the LETG calibration group to observe the target again for a more modest 120 ks. Observations were completed last October—well before all this polar vortex business started—and we have been comparing the data obtained at the two different epochs. Cozy optimism that our recalibration of the HRC-S QE using the Mkn 421 and HZ43 data would be vindicated was soon chilled by the impertinent polar vortex-like intrusion of the actual results that indicated a flux discrepancy of a few percent in the troublesome 30–60 Å range. It seems the QE correction we applied to this range was too large, suggesting that the relevant areas of the detector for those wavelengths did not respond to the voltage increase as much as the areas serving the shorter and longer wavelengths. This is probably nothing to do with the polar vortex, but more likely the spatial gain variation over the plates themselves.

While all the work following the voltage change to re-calibrate the HRC QE was underway, the other instrument teams did not sit politely by and wait for us to finish. Oh no. Rather, progress was brashly flaunted in a whirlwind of activity, like a polar vortex except a bit warmer, with updated HETG grating diffraction efficiencies, and a revised ACIS contamination model that reflects the more accurate emerging picture of the spatial and temporal evolution of the layer.
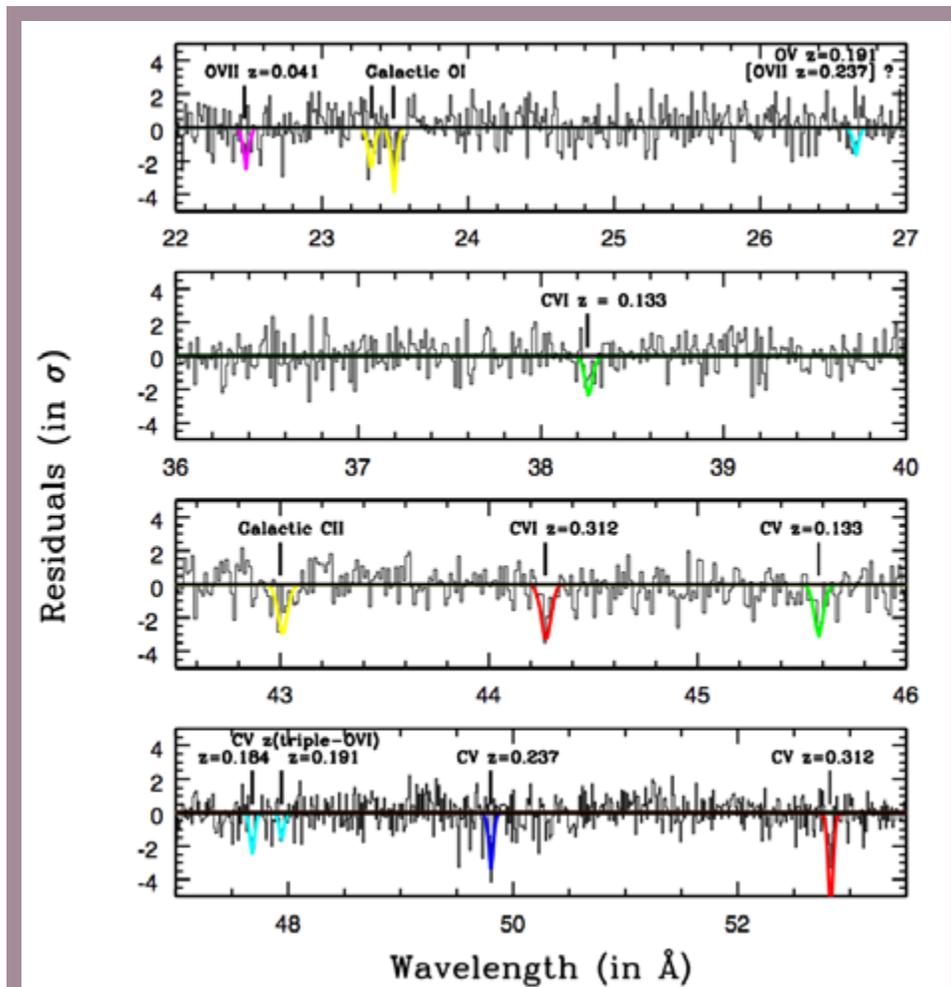

Fig. 2 — Residuals from a fit of the 500 ks LETG+HRC-S spectrum of the blazar 1ES 1553+113 to a continuum model. Galactic O I and C II are detected, as well as lines due to C V and C VI in different filaments of the WHIM. From Nicastro et al. (2013).

The LETG+HRC-S has only been absolutely calibrated in-flight, and then only at wavelengths longward of 50 Å or so where our white dwarf calibrators remain bright. At shorter wavelengths, the calibration has been tied to that of the MEG+ACIS-S combination. When any aspect of the calibration of this combination is changed, there is a knock-on effect through to the LETGS and any pleasant cordial concord between instruments, with their different colorful flux symbols overlapping nicely on plots, can be blown away, like colorful flux symbols on plots being blasted by an icy polar vortex. Current assessment of the flux symbols suggest the LETG+HRC-S ones are riding a little bit low at wavelengths shortward of 30 Å—perhaps about 10% lower than the ones in other colors representing the different instrument combinations. Reconciliation likely then requires a slight decrease in the higher energy HRC-S QE.

The two main components of the LETGS calibration are the detector quantum efficiencies and the diffraction efficiencies of the LETG itself. The latter are currently described by a diffraction model in first order, and empirically-derived corrections to the model for the higher orders. Convincing evidence indicating that the model for first order diffraction needs significant revision has so far been lacking, the matter being complicated by uncertainties in the time-dependent transmittance of the ACIS contamination layer, the lack of constant point-like calibration sources at higher energies, and earlier evidence that MEG and HEG diffraction efficiencies needed reconciling. With those elements now in place, for this iteration at least, we will soon be in a position to make a judgment on whether the first order efficiency requires correction. And so the cycle of calibration continues—just like a polar vortex, except different.

Still Warm

The LETGS has continued to defy the polar vortex by observing the absorbers in Seyfert galaxies, that remain warm, and the positively toasty warm-hot intergalactic medium. The warm absorbers in active galaxies are thought to originate as the wind driven from the hot central accreting vortex (some stubborn people still say "disk") around a supermassive black hole source. The outflows inject mass and energy into the host galaxy's interstellar medium at rates that might be sufficiently powerful to impact the evolution of the galaxy itself.

Combining LETG spectra from *Chandra* with data from *XMM-Newton* and HST on the Seyfert NGC 4593, Ebrero et al. (2013) found four distinct ionized plasma components, all outflowing at velocities of several hundreds of km per second. Fig. 1 shows the LETG spectrum in the 5–20 Å range in which absorption lines due to highly ionized Si, Ne, O and Fe are prominent. The outflowing gas responsible for this absorption was found to lie within 6–29 pc of the central ionizing source. Ebrero et al. (2013) were able to combine the velocity and absorption measurements to probe the total energy in the outflow. In this case, the kinetic energy of the outflows injected into the surroundings of the host galaxy were found to account for only a very small fraction of the total bolometric luminosity of the central source. The authors conclude that it is unlikely that the outflow has a significant impact on the interstellar medium of NGC 4593 in a single given episode of activity. Now, if it only had a polar vortex…

Instead of polar vortices, though, galaxies are thought only to have much more mundane "superwinds." These superwinds arise from supernova explosions and the outflows from active galactic nuclei, and perhaps contribute significant gas and metals to the warm-hot intergalactic medium (WHIM) that is predicted to host all those baryons that seem to have gone missing in the present epoch compared with the high-redshift universe (e.g. Cen & Ostriker 2006). Nicastro et al. (2013) have been looking for the baryons with *Chandra* again, trying to spot a few of them in the line-of-sight toward the blazar 1ES 1553+113. The experiment is simple enough—the blazar acts like a background continuum source against which the baryons should be seen in absorption, bathed in the blazar light and with their hands raised meekly in surrender. Nicastro et al. (2013) observed 1ES 1553+113 for 500 ks using the LETG+HRC-S and identified a total of 11 possible absorption lines, illustrated in residual form in Fig. 2. Three were from friendly Galactic baryons in the form of O I and C II, but five of the remaining eight appear to arise from C V and C VI Kα absorption in three distinct WHIM systems at redshifts between 0.133 and 0.312. These systems have also been detected in the far ultraviolet in H I and O VI absorption, and the authors suggest that the intergalactic medium structure could be more rich in ionization phase than typically predicted by cosmological hydrodynamic simulations (that, it must be pointed out, currently do not include the effect of the polar vortex).

JJD thanks the LETG team for useful comments, information and discussion.

References

Burwitz, V., Haberl, F., Neuhäuser, R., Predehl, P., Trümper, J., & Zavlin, V. E. 2003, A&A, 399, 1109

Cen, R., & Ostriker, J. P. 2006, ApJ, 650, 560

Drake, J. J., et al. 2002, ApJ, 572, 996

Ebrero, J., Kaastra, J. S., Kriss, G. A., de Vries, C. P., & Costantini, E. 2013, MNRAS, 435, 3028

Nicastro, F., et al. 2013, ApJ, 769, 90

Sartore, N., Tiengo, A., Mereghetti, S., De Luca, A., Turolla, R., & Haberl, F. 2012, A&A, 541, A66

Tiengo, A., & Mereghetti, S. 2007, ApJ, 657, L101

Chandra Calibration

Larry David

There were six releases of the *Chandra* calibration database (CALDB) during 2013. In addition to the regularly scheduled updates to the detector gains (quarterly for ACIS and yearly for the HRC), a new set of ACIS blank sky images were released, appropriate for data taken since 2009. An update to the ACIS contamination model also was released in November 2013 to account for changes over the past few years in the build-up rate, spatial distribution and chemical composition of the molecular contaminant that has been condensing onto the ACIS filters since launch. The build-up of molecular contaminant on the ACIS filters primarily affects the ACIS effective area below 2 keV. Based on periodic LETG/ACIS-S observations of blazars and ACIS imaging observations of the rich cluster Abell 1795, the condensation rate of the contaminant onto the optical filters began accelerating around 2009 and the optical depth of the contaminant has been increasing roughly linearly ever since. At about the same time, the chemical composition of the molecular contaminant also changed. These changes suggest that a different, more oxygen rich, contaminant is now condensing onto the ACIS filters. As of December 2013, the optical depth at 700 eV near the ACIS-I and ACIS-S aim-points is 1.3 (i.e., a transmission of 27%). The optical depth of the contaminant has always increased from the center to the edges of the ACIS detectors. In recent years, the difference between the optical depth at the detector edges and aim-points has accelerated. As of December 2013, the optical depth at 700 eV near the ACIS detector edges is 2.1 (i.e., a transmission of 12%). The most recent ACIS model is a pure elemental model and only includes absorption by carbon, oxygen and fluorine (i.e.,

the edges detected in gratings spectra) and accounts for the recent changes in the build-up rate, spatial distribution and chemical composition. A new calibration file to model the absorption was released by the CXC calibration group in the 4.5.9 release of the *Chandra* Calibration Database (CALDB) on 19 November 2013.

The *Chandra* calibration team continues to support the efforts of the International Astronomical Consortium for High Energy Calibration (IACHEC). These meetings bring together calibration scientists from all present and many future X-ray and γ-ray missions. Collaborations established at these meetings have led to a number of cross-calibration papers published in the Journal of Astronomy & Astrophysics. The next IACHEC meeting is scheduled for May 12–15, 2014 in Warrenton, Virginia.

Useful *Chandra* Web Addresses

To Change Your Mailing Address:
http://cxc.harvard.edu/cdo/udb/userdat.html

CXC:
http://chandra.harvard.edu/

CXC Science Support:
http://cxc.harvard.edu/

CXC Education and Outreach:
http://chandra.harvard.edu/pub.html

Science Publication Guidelines
http://cxc.harvard.edu/cdo/scipubs.html

ACIS: Penn State
http://www.astro.psu.edu/xray/axaf/

High Resolution Camera:
http://hea-www.harvard.edu/HRC/HomePage.html

HETG: MIT
http://space.mit.edu/HETG/

LETG: MPE
http://www.mpe.mpg.de/xray/wave/axaf/index.php

LETG: SRON
http://www.sron.nl/divisions/hea/chandra/

CIAO:
http://cxc.harvard.edu/ciao/

Chandra Calibration:
http://cxc.harvard.edu/cal/

MARX simulator
http://space.mit.edu/ASC/MARX/

MSFC: Project Science:
http://wwwastro.msfc.nasa.gov/xray/axafps.html

CIAO in 2013

The 4.6 release, brand new analysis scripts, a workshop, and some tips and tricks.

Antonella Fruscione, for the CIAO Team

Version 4.6 of CIAO and CALDB 4.5.9, the newest versions of the *Chandra* Interactive Analysis of Observations software and the *Chandra* Calibration Database, were released in November/December 2013. A small patch to the Sherpa package, CIAO 4.6.1, was later released in February 2014.

CIAO 4.6 (http://cxc.harvard.edu/ciao) includes numerous enhancements and bug fixes with respect to previous CIAO versions, all listed in detail in the software release notes. We will describe here some of the most notable changes and improvements. CIAO 4.6 is available for several 32 and 64 bit platforms including Linux CentOS 5 & 6 and Fedora Core 11, and Mac OSX 10.6.8 (Snow Leopard), 10.7 (Lion), 10.8 (Mountain Lion) and the latest 10.9 (Mavericks).

CIAO Tools

Two new tools have been added to help automate the detection of the 0th order location in grating observations: `tg_choose_method` and `tgdetect2`. The zeroth order of a *Chandra* grating observation defines the origin of the dispersed spectrum's wavelength scale. Hence, accurate determination of the zeroth order centroid is a fundamental step in the processing of grating data. The ACIS detector, however, can become saturated by bright sources. The brighter the source, the greater the distortion of the zeroth order due to rejection of core events, eventually leading to a "cratered" central region with few or no events. To mitigate telemetry saturation for observations of extremely bright sources, ACIS itself is sometimes configured to exclude the zeroth order from telemetry. In these distorted or blocked zeroth order cases the tgdetect tool fails to give an accurate result and the `tg_findzo` tool needs to be used instead. The new `tgdetect2` tool bundles three programs, `tg_choose_method`, `tg_findzo,` and `tgdetect`, into one so that the most appropriate method is chosen and used for the 0th order determination.

The suite of hotpixel tools, `acis_run_hotpix`, `acis_find_hotpix`, and `acis_classify_hotpix`, has been withdrawn from CIAO. The `acis_find_afterglow` tool is now considered the best tool available to identify cosmic ray afterglows without losing a large fraction of events from bright sources.

The ACIS parameter-block filename parameter, `pbkfile`, in `mkarf`, `mkgarf`, `mkwarf`, `eff2evt`, and `mean_energy_map` is no longer used. The information from this file, used in those tools, is now encoded in all the data products in the *Chandra* archive, which have been processed with the Standard Data Processing pipeline ASCDSVER 8.4.2 and later. It is also properly encoded in data that have been reprocessed with the `chandra_repro` script. So, there is one less input file that users need to carry around: the `acis*pbk*.fits` file is no longer needed for analysis.

Users with older data who choose not to reprocess their data, can use the new `r4_header_update` script to update the header; this will be done automatically if `chandra_repro` is run.

Sherpa

Sherpa (http://cxc.harvard.edu/sherpa/) is the modeling and fitting application within CIAO and can be used for analysis of images, spectra and time series from many telescopes, including optical telescopes such as *Hubble*. Sherpa is flexible, modular and extensible. It has an IPython user interface and it is also an importable Python module. Sherpa models, optimization, and statistical functions are available via both Python and C++ for software developers wishing to link such functions directly to their own code. Important changes and additions to the Sherpa functionality in the CIAO 4.6 release and 4.6.1 patch are described in a dedicated webpage at http://cxc.harvard.edu/sherpa/updates.html.

The most notable improvement in the CIAO 4.6 Sherpa release concerns template models (http://cxc.harvard.edu/sherpa/threads/template_model/). The Sherpa template model is available for comparing a source data spectrum against a set of user-provided template models, in order to find the single template model which best matches the source data. Generally a special grid-search fit optimization method, `gridsearch`, is used to fit a template model to a data set in Sherpa— however CIAO 4.6 adds the ability to use templates with fitting methods other than `gridsearch`. Starting with a directory of template model files conforming to a specific format, and a single index file listing the file contents of that directory, the models are loaded into the Sherpa session using the `load_template_model`

function, an extension of `load_table_model`. After fitting the template model to the source data using the fit optimization method, the parameters of the best-match template model are returned. Fit results may be examined in the usual way with the appropriate plotting commands. The Sherpa template model supports linear, nearest-neighbor, and polynomial interpolation. Interpolation is used by the template model to match the data grid to the model grid, which must match before the fit statistics can be calculated for fitting.

CIAO 4.6 introduces the ability to interpolate between templates loaded with the `load_template_model` function, so that intermediate parameter values may be found during a fit. It also adds the ability to use templates with fitting methods other than gridsearch and to combine templates with other Sherpa models, and fit on all parameters (from both the template and the continuous models).

ChIPS

ChIPS (http://cxc.harvard.edu/chips/) is the imaging and plotting platform for CIAO which can be used during data analysis—e.g. to plot a lightcurve or a spectrum—and to create publication-quality figures. ChIPS is designed for use in a variety of modes: as a user-interactive application and in batch mode. ChIPS is an importable module for the Python scripting language and is available as a C/C++ library for software developers.

The CIAO 4.6 release of ChIPS does not include any major new functionality but several minor enhancements and bug fixes. A large gallery of ChIPS examples is available on the ChIPS website at http://cxc.harvard.edu/chips/gallery/ and there are a number of introductory threads to guide beginners.

CIAO Scripts

The CIAO contributed scripts package (http://cxc.harvard.edu/ciao/download/scripts/) is considered a required part of the software installation and contains analysis scripts and modules written by scientists at the CXC. The contributed scripts and modules automate repetitive tasks and extend the functionality of the CIAO software package by filling specific analysis needs. The package is updated every few months or as needed, and also concurrently with major CIAO releases. During 2013 there were 4 script package releases bringing in some major new functionality and important enhancements, all listed at http://cxc.harvard.edu/ciao/download/scripts/history.html. A few important scripts are highlighted below.

`srcflux`: given an event file and a location, this script calculates the net count rates and fluxes, including uncertainties, using three different methods. The count rate is calculated using the `aprates` tool, and so can be used to estimate upper limits as well as detections, and—for point sources—to account for the PSF contribution to both the source and background regions. The flux is estimated in three ways:
- a model-independent estimate, using the `eff2evt` tool
- a model-dependent estimate, using the `modelflux` tool to calculate the conversion factor for a given spectral model (for this stage ARFs and RMFs will be created for each source).
- in photon units by using the `fluximage` tool to create exposure map and exposure corrected image.

The analysis thread "Calculate Source Count Rates and Fluxes" (http://cxc.harvard.edu/ciao/threads/fluxes/) has examples on how to use this new script as well as tips in case of problems.

Example output from `srcflux` operating on an event file.

```
unix% srcflux acisf13459_repro_evt2.fits "0:55:51.013 +26:22:43.95" myout
[...]
Summary of source fluxes


Position                              0.5-7.0 keV
                                      Value    90% Conf Interval
0 55 51.01 +26 22 43.9   Rate         0.00191c/s (0.00168,0.00214)
                         Flux         2.27E-14 erg/cm2/s (2E-14,2.55E-14)
                         Mod.Flux     2.43E-14 erg/cm2/s (2.14E-14,2.73E-14)
```
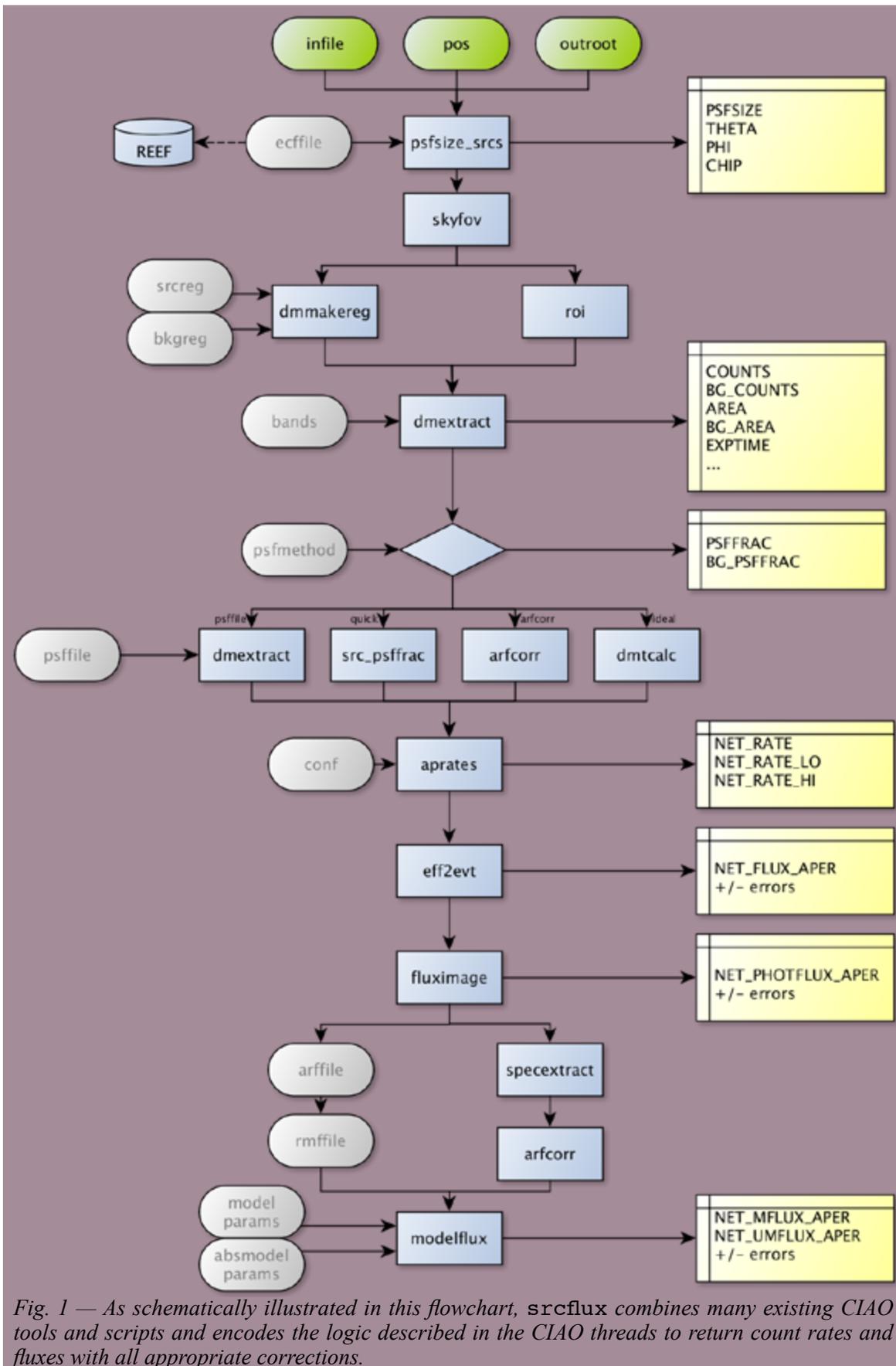
Fig. 1 — As schematically illustrated in this flowchart, **srcflux** combines many existing CIAO tools and scripts and encodes the logic described in the CIAO threads to return count rates and fluxes with all appropriate corrections.

The following search will retrieve all the default source properties for all the sources detected in ObsID 635 (RhoOph). The output columns are saved in a Tab Separated Value (TSV) file and includes properties such as position, fluxes, extent, and measures of variability. Additionally, the spectrum (pha) files and the associated response files (ARF and RMF) for each source will optionally be downloaded (only the first source is downloaded in this example).

```
unix% obsid_search_csc 635 outfile=rhooph.tsv verb=0 filetype=pha,rmf,arf download=ask
Download data for CXO J162602.2-242348 in 00635_000 [y,n,a,q]: y
Download data for CXO J162603.1-242336 in 00635_000 [y,n,a,q]: q
Skipping remaining sources

unix%  ls -1 635/CXOJ162602.2-242348/
acisf00635_000N001_r0067_arf3.fits.gz
acisf00635_000N001_r0067_pha3.fits.gz
acisf00635_000N001_r0067_rmf3.fits.gz
```

The spectrum file that is retrieved can be loaded directly into Sherpa for analysis. The background spectrum is automatically recognized as being located in the second extension of the PHA file. The response files are also automatically recognized.

```
unix% sherpa
------------------------------------------------------
Welcome to Sherpa: CXC's Modeling and Fitting Package
------------------------------------------------------
CIAO 4.6 Sherpa version 1 Monday, December 2, 2013

sherpa-1> load_data("635/CXOJ162602.2-242348/acisf00635_000N001_r0067_pha3.fits.gz")
read ARF file 635/CXOJ162602.2-242348/acisf00635_000N001_r0067_arf3.fits
read RMF file 635/CXOJ162602.2-242348/acisf00635_000N001_r0067_rmf3.fits
read background file 635/CXOJ162602.2-242348/acisf00635_000N001_r0067_pha3.fits
sherpa-2> plot_data()
```

The source properties are stored in the TSV output file, rhooph.tsv. Thanks to the DM's ASCII kernel, this file can be read into all CIAO applications. Users simply need to specify the specific ASCII format, [opt kernel=text/tsv], due to its unique header structure. Shown here is how to simply plot two columns using ChIPS.

```
unix% chips
-----------------------------------------
Welcome to ChIPS: CXC's Plotting Package
-----------------------------------------
CIAO 4.6 ChIPS version 1 Monday, December 2, 2013
chips-1> make_figure("rhooph.tsv[opt kernel=text/tsv][cols cnts_aper_b,flux_significance_b]")
chips-2> show_gui() → to customize the plot
```
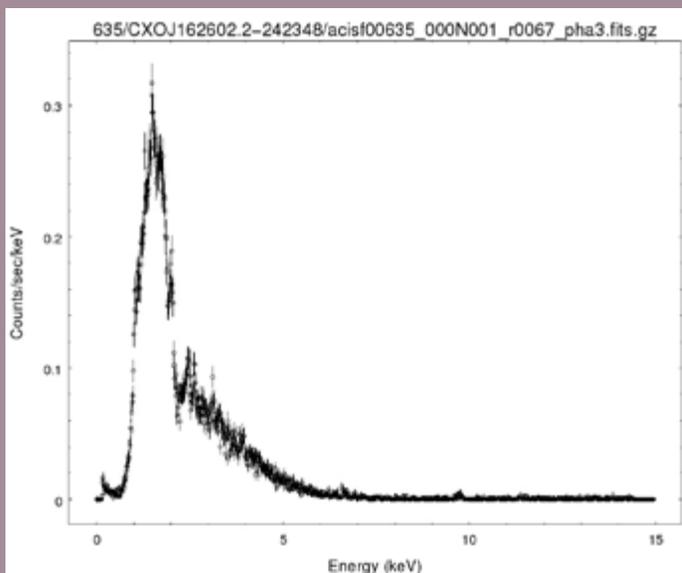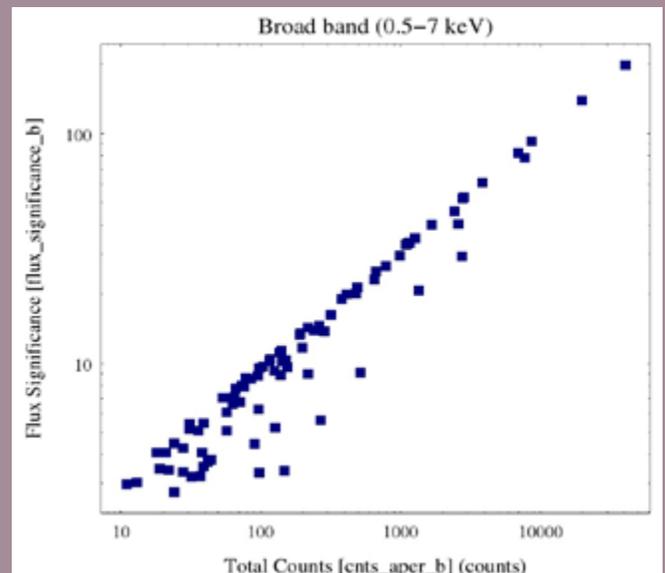
Fig. 2 — Sherpa example output   *Fig. 3 — ChIPS example output*

search_csc and obsid_search_csc: these scripts allow full command line access to the *Chandra* Source Catalog (CSC), with simple search capabilities. Searches can be accomplished by position or by obsid with access to all the Master and all the Observations properties.

Both scripts can retrieve arbitrary sets of columns from the CSC and save the results as a tab-delimited ASCII file that can be used directly with other CIAO applications. Additionally, the per source and per observation data products—including event files; images; spectra; lightcurves; and their associated response files (PSF, RMF, ARF, exposure maps) may be retrieved.

The thread *Simple Command Line Access to the Chandra Source Catalog* (http://cxc.harvard.edu/ciao/threads/csccli/) illustrates the usage of these new scripts.

tgmask2reg and reg2tgmask: these scripts allow the use of DS9 to define custom extraction regions for HRC grating observations to be used with the tgextract2 tool which provides support for variable-shaped background regions (see the thread "*Applying Customized Background Regions to LETG/HRC-S Observations*" at http://cxc.cfa.harvard.edu/ciao/threads/tgextract2/)

mktgresp: this script creates ARF and RMF for each spectral order and grating arm in a Type II PHA file. It runs the mkgrmf tool and the fullgarf script with the appropriate inputs using the energy and channel grids. For ACIS data, the default PHA files has 12 spectra for HETG: ± 3 orders for each MEG and HEG, and 6 for LETG: ± 3 orders. Since HRC lacks energy resolution, the spectra cannot be order separated so there are only 2 spectra: ± 1 which represents the contribution from all orders. A corresponding number of responses files are created by mktgresp.

dax (ds9 analysis extensions): a number of common CIAO tasks are available from the ds9 Analysis menu. This menu addition allows users to get source counts, smooth an image, and create a histogram—among many other things—from the ds9 program in CIAO. A number of new tasks are available in CIAO 4.6 dax: a Sherpa menu to automatically fit some simple 1D and 2D models, aperture photometry, period fold, convex hull, PSF size and fraction, distance transform and image moments. Several YouTube demos (http://www.youtube.com/playlist?list=PLE60ED562991C612E) illustrate the use of dax in ds9.

psfsize_srcs and src_psffrac: these scripts (a) compute the size of a circle that encloses the specified fraction of the PSF at the specified energy for each of the input positions or (b) compute an approximate value of the fraction of the PSF in circular regions at the specified monochromatic energy.

list_datasetid: this script provides the LaTeX identifier macro used to describe observations in papers written for AAS managed publications. The CXC encourages users to make use of dataset identifiers when publishing in AAS managed publications. This allows the publisher, through agreement with the *Chandra* Data Archive as well as other archives, to provide links to the actual datasets within their document. This makes it easier for readers to locate the data being reported on in the manuscript.

Fig. 2 — The 9th Chandra/CIAO workshop

9th CIAO Workshop

The 9th *Chandra*/CIAO workshop was held on April 23 and 24, 2013 at the Harvard-Smithsonian Center for Astrophysics in Cambridge, MA. It was 2 days of hands-on work with one introductory talk on CIAO and the recent advancements in CIAO scripts. Sample analysis exercises were provided for students, who were also encouraged to bring their own data if they had any: some students arrived with specific problems or questions in hand, while others were beginners just getting started with CIAO for the first time.

From the feedback we received, the workshop was productive for attendees and was certainly very useful for us for improving our existing on-line documentation.

Tips, Tricks, and Techniques

Most of the CIAO analysis threads (http://cxc.harvard.edu/ciao/threads/all.html) are focused on a particular science goal or objective: instrument, grating, point source vs. extended, etc. They present the best path to reduce the data for those specific goals. However, there are many kinds of analysis techniques that apply to general data reduction that can be performed with CIAO—on *Chandra* data or other missions.

The threads presented in this new section of the CIAO threads "Tips, Tricks and Techniques"—TTT (http://cxc.harvard.edu/ciao/threads/ttt.html) will focus on *how* to accomplish a particular task and the options available. *When* one should use these techniques, and *why* one might want to do such a thing is up to the user. The emphasis is to highlight the functionality available. We are expecting that users will find uses for CIAO that the CXC might not have anticipated.

More information and updates on CIAO can always be found at http://cxc.harvard.edu/ciao/ or subscribe to the CIAO News RSS feed at http://cxc.harvard.edu/ciao/feed.xml The latest tutorials, demos, and screen-casts of CIAO are available onthe "4ciaodemos" channel at http://www.youtube.com/user/4ciaodemos

To keep up-to-date with CIAO news and developments subscribe to the *Chandra* Electronic Announcements at http://cxc.harvard.edu/announcements/.

Einstein Postdoctoral Fellowship Program

Andrea Prestwich

The Call for Proposals for the 2014 class of Einstein Fellows was released in July 2013. This is the 6th year of the Einstein Fellowship Program, which started in 2008 with the combination of the *Chandra* and Fermi Fellowship programs. Interest in the program remains very high with 185 applications for 12 Fellowships. The Fellowship Selection Panel met January 15-16, and all candidates received a "sorry," "wait list," or "offer" email on the afternoon of January 16. At the time of writing (January 2014) finalists are considering their offers. We expect the 2014 class to be finalized by mid-March, with the list posted to http://cxc.harvard.edu/fellows/. The 2013 Fellowship Symposium was held in October here at the Harvard-Smithsonian Center for Astrophysics (CfA). The talks were terrific and much-enjoyed by scientists from the CfA and other institutions in the vicinity.

Einstein Fellows have had some notable successes this year. Meng Su (Class of 2012) was awarded the AAS High Energy Astrophysics Division Bruno Rossi Prize with Douglas Finkbeiner (Harvard-Smithsonian Center for Astrophysics) and Tracy Slatyer (MIT) for their discovery of the "Fermi Bubbles." Jennifer Siegal-Gaskins (Class of 2011) was awarded a Marie Curie (Incoming International Fellow) Fellowship and Amy Reines (Class of 2011) is starting a Hubble Fellowship at the University of Michigan in the fall. Smadar Naoz (Class of 2012) has accepted a faculty position at the University of California, Los Angles and Claude-Andre Faucher-Giguere at Northwestern University. Smadar Naoz had a paper published in Physics Review Letters that was featured as a "Physics Viewpoint" article, and work by Amy Reines on supermassive black holes in dwarf galaxies was the subject of a press release at the American Astronomical Society.

In addition to their busy professional lives, several Fellows celebrated personal milestones. Rutger van Haasteren married violinist Olga D. Katkova on December 5, 2013. Joey Neilson and his wife Kate are the proud parents of Owen Oliver Neilson (born 11 December 2013) and Radoslaw Nalewajko was born on July 23 2013 just 7 days before his papa Krzysztof Nalewajko started his Fellowship at the University of Colorado at Boulder!

Cycle 15 Peer Review Results

Belinda Wilkes

The observations approved for *Chandra*'s 15th observing cycle are now in full swing and the Cycle 16 Call for Proposals (CfP) was released on 12 December 2013. Cycle 14 observations are close to completion.

The Cycle 15 observing and research program was selected as usual, following the recommendations of the peer review panels. The peer review was held 18−21 June 2013 at the Hilton Boston Logan Airport. It was attended by 110 reviewers from all over the world, who sat on 15 panels to discuss the 636 submitted proposals (Fig. 1). The "Target Lists and Schedules" link of our website (http://cxc.harvard.edu/target_lists/) provides access to lists of the various approved programs, including abstracts. The peer review panel organization is shown in Table 1.

The Cycle 15 CfP included a third call for X-ray Visionary Projects (XVPs). XVPs are major, coherent science programs to address key, high-impact scientific questions in current astrophysics. The amount of time available for XVPs was reduced to 5 Ms this cycle. The continuing, expected evolution of *Chandra*'s orbit is decreasing the amount of "additional" available observing time, because the fraction of each orbit spent within the radiation belts is increasing. The total amount of time allocated in Cycle 15 was 20 Ms, including 5 Ms awarded to 2 XVPs and 3.6 Ms to 8 LPs. The response to the XVP opportunity continued to be very strong, with over-subscriptions in telescope time for LPs and XVPs of 8.8 and 6.4 respectively. The overall over-subscription in observing time was

Topical Panels:	
Galactic	
Panels 1,2	Normal Stars, WD, Planetary Systems and Misc
Panels 3,4	SN, SNR + Isolated NS
Panels 5,6,7	WD Binaries + CVs, BH and NS Binaries, Galaxies: Populations
Extragalactic	
Panels 8,9,10	Galaxies: Diffuse Emission, Clusters of Galaxies
Panels 11,12,13	AGN, Extragalactic Surveys
XVP Panel	X-ray Visionary Proposals
Big Project Panel	LP and XVP Proposals

Table 1: Panel Organization

5.3 (Fig. 2), typical of the past few cycles despite the larger amount of time being requested and allocated (Fig. 3). As the continued evolution of the *Chandra* orbit brings it back to a more typical configuration, the smaller amounts of excess time in Cycles 16, 17 are being combined to provide a pool of 5 Ms which will be allocated in Cycle 16 and observed over both cycles. There will be no XVP call in Cycle 17.

Following our standard procedure, all proposals were reviewed and graded by the topical panels, based primarily upon their scientific merit, across all proposal types. The topical panels were allotted *Chandra* time to cover the allocation of time for GO observing proposals based upon the demand for time in each panel. Other allocations made to each panel included: joint
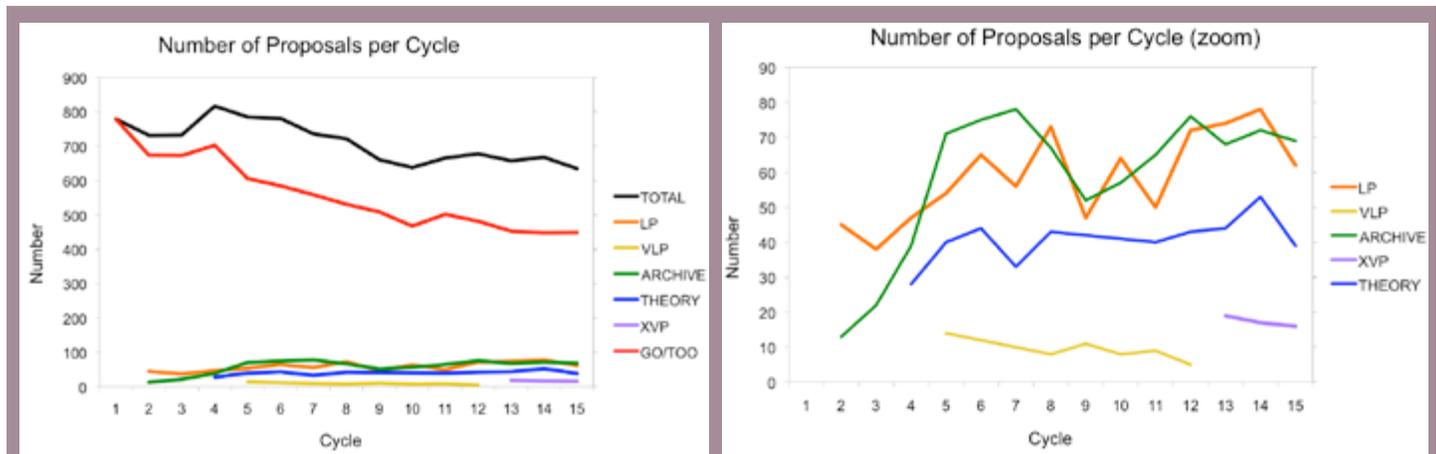

Fig. 1 — a: The number of proposals submitted in each proposal category (e.g. GO, LP, Archive etc.) as a function of cycle, b: zoom on lower curves. Since more proposal categories have become available in each cycle, the number classified as GO has decreased as others increased. The total number of submitted proposals has been remarkably constant over the past 8-9 cycles.
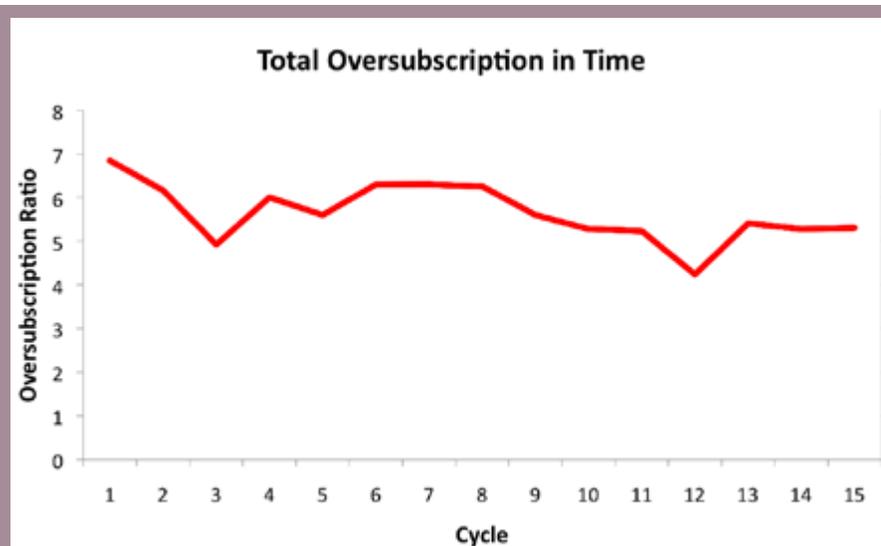
Fig. 2 — The final over-subscription in observing time based on requested and allocated time in each cycle. The numbers are remarkably constant. The decrease in Cycle 12 reflects the late, 16% increase in the amount of time awarded by the peer review in that cycle to offset the significantly increased observing efficiency as the orbit evolved (see article in 2011 Newsletter).

time, TOOs with a < 30 day response, time constrained observations in each of 3 constraint classes, time in future cycles, constrained observations in future cycles, and money to fund archive and theory proposals. These allocations were based on the full peer review over-subscription ratio. The topical panels produced a rank-ordered list along with detailed recommendations for individual proposals where relevant. A report was drafted for each proposal by one/two members of the appropriate topical review panel and reviewed by the Deputy panel chair before being delivered to the CXC. Panel allocations were modified, either during the review or in some cases after its completion, to transfer unused allocations between panels so as to follow the review recommendations as closely as possible.

LPs and XVPs were discussed by the topical panels and ranked along with the GO, archive and theory proposals. In addition, the XVPs were discussed and ranked by a separate XVP/pundit panel. The topical and XVP panels' recommendations were recorded and passed to the Big Project Panel (BPP), which included all topical panel chairs and members of the XVP panel. The schedule for the BPP at the review included time for reading

and for meeting with appropriate panel members to allow coordination for each subject area. The BPP discussed the LPs and XVPs separately and generated two rank-ordered proposal lists. The meeting extended into Friday afternoon to allow for additional discussion, for a consensus on the final rank-ordered lists to be reached, and to ensure that all observing time was allocated. At least 2 BPP panelists updated each review report to include any BPP discussion, at the review and/or remotely over the following week.

The resulting observing and research program for Cycle 15 was posted on the CXC website on 12 July 2013, following detailed checks by CXC staff and approval by the Selection Official (CXC Director).

All peer review reports were reviewed by CXC staff for clarity and consistency with the recommended target list. Budget allocations were determined for proposals which included US-based investigators. Formal e-letters informing the PIs of the results, budget information (when appropriate) and providing the report from the peer review, were e-mailed to each PI in August.
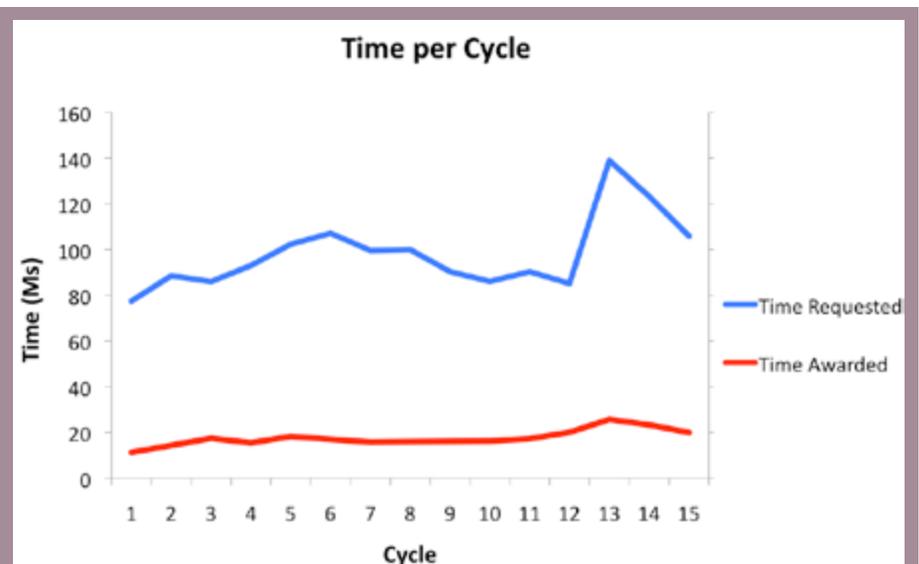

Fig. 3 — The requested and approved time as a function of cycle in Ms including allowance for the probability of triggering each TOO. The available time increased over the first 3 cycles, and in Cycle 5 with the introduction of Very Large Projects (VLPs). The subsequent increase in time to be awarded due to the increasing observing efficiency and the corresponding increase in requested time in response to the calls for X-ray Visionary Projects (XVPs) in Cycles 13-15 is clear.
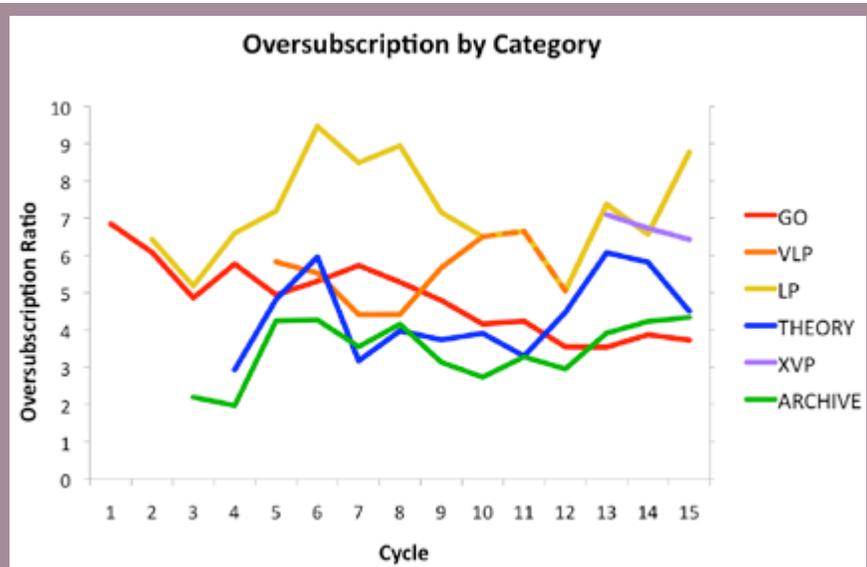
Fig. 4 — The effective over-subscription ratio in terms of observing time for each proposal category as a function of cycle. Note that some of the fluctuations are due to small number statistics (e.g. Theory proposals).

Joint Time Allocation

Chandra time was also allocated to several joint programs by the proposal review processes of *XMM-Newton* (1 proposal), Spitzer (1 proposal), and HST (1 proposal). The *Chandra* review accepted joint proposals with time allocated on: Hubble (11), *XMM-Newton* (4), Swift (3), NRAO (13), and NOAO (2).

Constrained Observations

As observers are aware, the biggest challenge to efficient scheduling of *Chandra* observations is in regulating the temperature of the various satellite components (see POG Section 3.3.3, and the ACIS article in this Newsletter). In Cycle 9 we instituted a classification scheme for constrained observations which accounts for the difficulty of scheduling a given observation (CfP Section 5.2.8). Each constraint class was allocated an annual quota based on our experience in previous cycles. The same classification scheme was used in Cycles 10-15. In Cycles 13-15 the quotas were increased, commensurate with the larger amount of observing time to be awarded. There was a large demand for constrained time so that not all proposals which requested time

constrained observations and had a passing rank (>3.5) could be approved. Effort was made to ensure that the limited number of constrained observations were allocated to the highest-ranked proposals review-wide. Detailed discussions were carried out with panel chairs to record the priorities of their panels in the event that more constrained observations could be allocated. Any uncertainty concerning priorities encountered during the final decision process was discussed with the relevant panel chairs before the recommended target list was finalized.

Please note that the most over-subscribed constraint class was "EASY" while "AVERAGE" was only marginally over-subscribed. In practice these two classes were combined when determining which observations should be allocated time. The same 3 classes will be retained in Cycle 16 so as to ensure a broad distribution in the requested contraints. *We urge proposers to request the class of constraint required to achieve the science goals.*
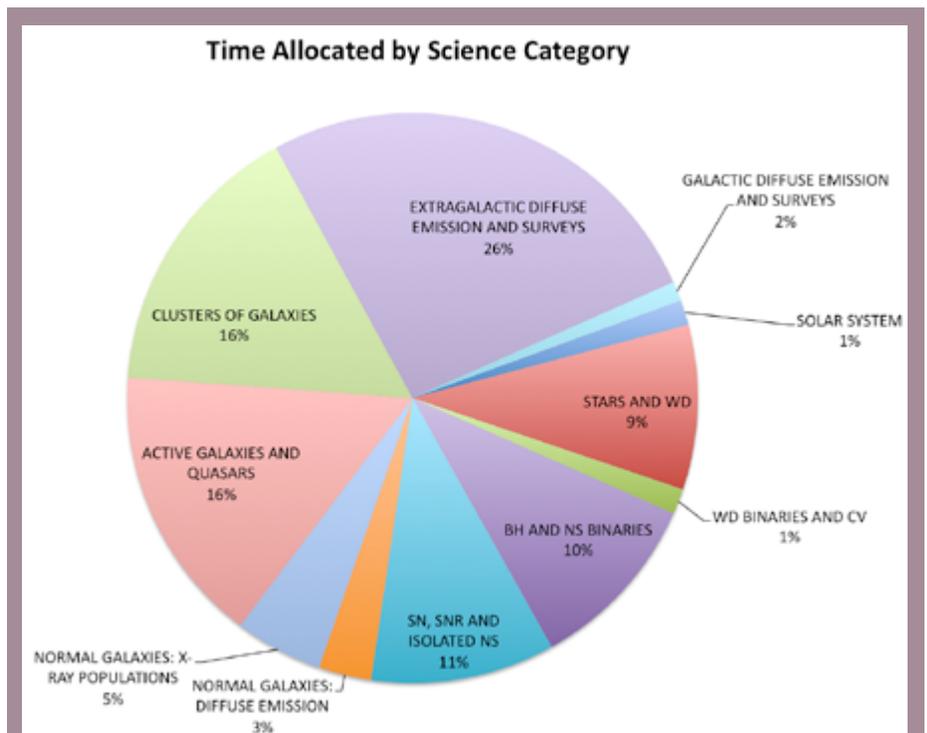

Fig. 5 — A pie chart indicating the percentage of Chandra *time allocated in each science category. Note that the time available for each science category is determined by the demand.*

Cost Proposals

PIs of proposals with US collaborators were invited to submit a Cost Proposal, due Sept 2013 at SAO. In Cycle 15 each project was allocated a budget based on the details of the observing program (see CfP Section 8.4). Awards were made at the allocated or requested budget levels, whichever was lower. The award letters were emailed in late November, in good time for the official start of Cycle 15 on 1 Jan 2014.

Given the uncertainty in the FY14 Federal (and thus NASA) budget, Cycle 15 award letters included notification that award amounts may be reduced if sequestration or other cuts are made to the NASA *Chandra* budget. All *Chandra* awards are initially being funded at 50% of the final award amount, with the remaining 50% to be issued in March now that the FY14 budget level has been confirmed.

Proposal Statistics

Statistics on the results of the peer review can be found on our website: under "Target Lists and Schedules," select the "Statistics" link for a given cycle. We present a subset of those statistics here. Fig. 4 displays the effective over-subscription rate for each proposal type as a function of cycle. Fig. 5 and 6 show the percentage of time allocated to each science category and to each instrument combination. Table 2 lists the numbers of proposals submitted and approved per country of origin.
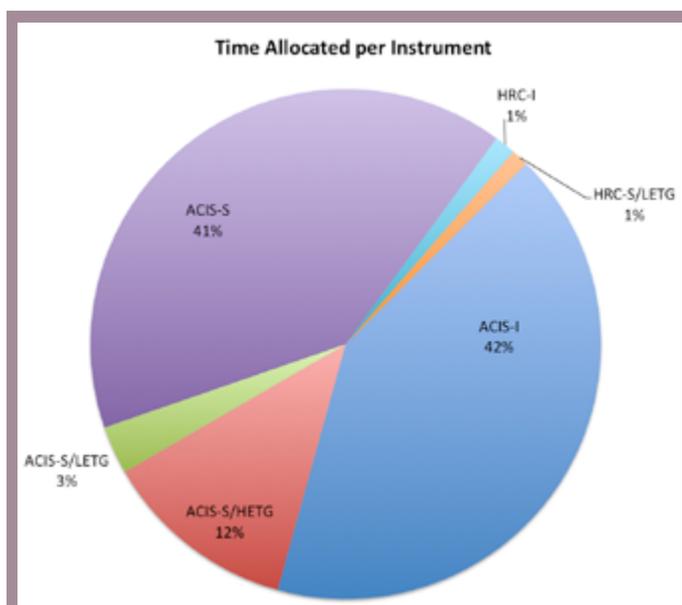

Fig. 6 — A pie chart showing the percentage of Chandra *time allocated to observations for each instrument configuration.*

Table 2: Number of Requested and Approved Proposals by Country

Country	Requested		Approved	
	# Proposals	Time (ks)	# Proposals	Time (ks)
USA	479	84309	137	17464
Foreign	157	24810	42	4315
Country	Requested		Approved	
	# Proposals	Time (ks)	# Proposals	Time (ks)
Australia	1	40	1	40
Belgium	1	350		
Bulgaria	1	139		
Canada	10	1405	2	195
Chile	2	230	1	190
China	2	185		
France	8	767	4	376
Germany	31	3453	8	1335
Greece	4	570	1	50
India	5	356	4	316
Ireland	1	21		
Israel	2	120	1	60
Italy	28	6985	7	651
Japan	12	1550	2	64
Korea	1	30		
Netherlands	11	1067	2	73
Poland	1	40		
Russia	2	42		
Slovakia	1	216		
Spain	6	960	2	165
Switzerland	2	530	1	250
Taiwan	5	340		
Turkey	1	20		
U.K.	19	5395	6	550

* Note: Numbers quoted here do not allow for the probability of triggering TOOs

Chandra Users' Committee Membership List

The Users' Committee represents the larger astronomical community for the *Chandra* X-ray Center.
If you have concerns about *Chandra*, contact one of the members listed below.

Name	Organization	Email
Lee Armus	SSC	lee@ipac.caltech.edu
Franz Bauer	SSI	fbauer@spacescience.org
Tiziana DiMatteo	CMU	tiziana@lemo.phys.cmu.edu
Erica Ellingson	CASA-Colorado	erica.ellingson@colorado.edu
Tim Kallman	GSFC	Timothy.R.Kallman@nasa.gov
Carol Lonsdale	NRAO	clonsdal@nrao.edu
Hironori Matsumoto	Nagoya University	matumoto@u.phys.nagoya-u.ac.jp
Jon Miller (Chair)	University of Michigan	jonmm@umich.edu
Rachel Osten	STScI	osten@stsci.edu
Feryal Ozel	University of Arizona	fozel@email.arizona.edu
Pedro Rodriguez	ESA	prodrigu@sciops.esa.int
Paul Martini	Ohio State University	martini@astronomy.ohio-state.edu
Ex Officio, Non-Voting		
Jeff Hayes	NASA HQ	jeffrey.hayes-1@nasa.gov
Larry Petro	NASA HQ	Larry.D.Petro@nasa.gov
Wilt Sanders	NASA HQ	wsanders@hq.nasa.gov
Allyn Tennant	NASA/MSFC, Project Science	allyn.tennant@msfc.nasa.gov
Martin Weisskopf	NASA/MSFC, Project Scientist	martin.c.weisskopf@nasa.gov
CXC Coordinator		
Paul Green	CXC Director's Office	pgreen@head.cfa.harvard.edu

CXC 2013 Press Releases

<div align="right">Megan Watzke</div>

Date	PI	Objects	Title
7 January	Martin Durant (Univ. of Toronto)	Vela Pulsar	New *Chandra* Movie Features Neutron Star Action
13 February	Laura Lopez (MIT)	W49B	NASA's *Chandra* Suggests Rare Explosion Created Our Galaxy's Youngest Black Hole
18 March	Mary Burkey (North Carolina State)	Kepler Remnant	Famous Supernova Reveals Clues About Crucial Cosmic Distance Markers
9 April	NASA/CXC	Einstein Fellows	2013 Einstein Fellows Chosen
23 May	Nanda Rea (Institute of Space Science, Barcelona)	SGR 0418+5729	A Hidden Population of Exotic Neutron Stars
12 June	Robin Barnard (CfA)	M31	NASA's *Chandra* Turns up Black Hole Bonanza in Galaxy Next Door
29 June	Katja Poppenhaeger (CfA)	HD 189733b	NASA's *Chandra* Sees Eclipsing Planet in X-rays for First Time
29 August	Q. Daniel Wang (UMass)	Sgr A*	NASA'S *Chandra* Catches Our Galaxy's Giant Black Hole Rejecting Food
24 September	Jay Strader (Michigan State)	M60-UCD1	NASA's Hubble and *Chandra* Find Evidence for Densest Nearby Galaxy
24 October	Christine Jones (CfA)	Frontier Fields	NASA's Great Observatories Begin Deepest Ever Probe of the Universe
20 November	Zhiyuan Li (Nanjing University, China)	Sgr A*	NASA's *Chandra* Helps Confirm Evidence of Jet in Milky Way's Black Hole
4 December	Julie Hlavacek-Larrondo (Stanford)	18 galaxy clusters	Supernova Blast Provides Clues to Age of Binary Star System

Links to all of these press releases can be found at http://www.chandra.harvard.edu/press/13_releases/

Additional image releases and other features that were issued during 2013 are available at:
http://www.chandra.harvard.edu/photo/chronological13.html

Credit: X-ray: NASA/CXC/CfA/D. Evans et al.; Optical/UV: NASA/STScI; Radio: NSF/VLA/CfA/D. Evans et al., STFC/JBO/MERLIN

The active galaxy 3C321 is shown in X-rays from *Chandra* (colored purple), optical and ultraviolet (UV) from *Hubble* (red and orange), and radio emission from the Very Large Array (VLA) and MER-LIN (blue) from Evans et al. (2008). See Fig. 7 of Aneta Siemiginowska's article inside.